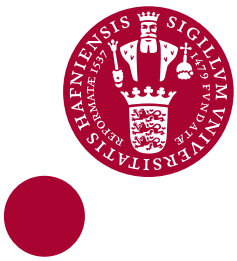

Phenomenology of GeV-scale heavy neutral leptons

Bondarenko, Kyrylo; Boyarsky, Alexey; Gorbunov, Dmitry; Ruchayskiy, Oleg

Published in:
Journal of High Energy Physics

DOI:
10.1007/JHEP11(2018)032

Publication date:
2018

Document version
Publisher's PDF, also known as Version of record

Published for SISSA by Springer

Received: *August 21, 2018*
Accepted: *October 17, 2018*
Published: *November 6, 2018*

Phenomenology of GeV-scale heavy neutral leptons

Kyrylo Bondarenko,[a] **Alexey Boyarsky,**[a] **Dmitry Gorbunov**[b,c] **and Oleg Ruchayskiy**[d]

[a] *Intituut-Lorentz, Leiden University, Niels Bohrweg 2, 2333 CA Leiden, The Netherlands*
[b] *Institute for Nuclear Research of the Russian Academy of Sciences, Moscow 117312, Russia*
[c] *Moscow Institute of Physics and Technology, Dolgoprudny 141700, Russia*
[d] *Discovery Center, Niels Bohr Institute, Copenhagen University, Blegdamsvej 17, DK-2100 Copenhagen, Denmark*

E-mail: bondarenko@lorentz.leidenuniv.nl, boyarsky@lorentz.leidenuniv.nl, gorby@inr.ac.ru, oleg.ruchayskiy@nbi.ku.dk

Abstract: We review and revise phenomenology of the GeV-scale heavy neutral leptons (HNLs). We extend the previous analyses by including more channels of HNLs production and decay and provide with more refined treatment, including QCD corrections for the HNLs of masses $\mathcal{O}(1)$ GeV. We summarize the relevance of individual production and decay channels for different masses, resolving a few discrepancies in the literature. Our final results are directly suitable for sensitivity studies of particle physics experiments (ranging from proton beam-dump to the LHC) aiming at searches for heavy neutral leptons.

Keywords: Beyond Standard Model, Heavy Quark Physics, Chiral Lagrangians

ArXiv ePrint: 1805.08567

https://doi.org/10.1007/JHEP11(2018)032

JHEP11(2018)032

Contents

JHEP11(2018)032

1 Introduction: heavy neutral leptons

We review and revise phenomenology of the heavy neutral leptons (HNLs) with masses in the GeV range. The interest to these particles has recently increased, since it was recognized that they are capable of resolving 3 major observational BSM phenomena: neutrino oscillation, baryon asymmetry of the universe and dark matter [1, 2] (for review see e.g. [3, 4], [5, Chapter 4] and references therein).

Several particle physics experiments, that put the searches for heavy neutral leptons among their scientific goals, have been proposed in the recent years: DUNE [6], NA62 [7–9] SHiP [5, 10], CODEX-b [11], MATHUSLA [12–15], FASER [16–18]. The searches for HNLs (also often called "Majorana neutrinos" or "sterile neutrinos") have been performed and are ongoing at the experiments LHCb, CMS, ATLAS, T2K, Belle (see e.g. [19–24]) with many more proposals for novel ways to search for them [25–48]. This interest motivates the current revision. The information relevant for sensitivity studies of the GeV-scale HNLs is scattered around the research literature [37, 39, 48–57] and is sometimes controversial. We collect all relevant phenomenological results and present them with the unified notation, discussion of the relevance of the individual channels and references to the latest values of phenomenological parameters (meson form factors) that should be used in practical application. The relevance of individual channels depending on the masses of HNLs is present in the resulting table 5. We also discuss existing discrepancies in the literature, pointing out the way of obtaining the correct results and analyze new channels of production and new modes of decay neglected in the previous literature.

JHEP11(2018)032

1.1 General introduction to heavy neutral leptons

Heavy neutral leptons or sterile neutrinos N are singlets with respect to the SM gauge group and couple to the gauge-invariant combination $(\bar{L}^c_\alpha \cdot \tilde{H})$ (where L_α, $\alpha = 1, \ldots, 3$, are SM lepton doublet, $\tilde{H}_i = \varepsilon_{ij} H^*_j$ is conjugated SM Higgs doublet) as follows

$$\mathcal{L}_{\text{Neutrino portal}} = F_\alpha (\bar{L}_\alpha \cdot \tilde{H}) N + h.c.\,, \tag{1.1}$$

with F_α denoting dimensionless Yukawa couplings. The name "sterile neutrino" stems from the fact that the interaction (1.1) fixes SM gauge charges of N to be zero. After electroweak symmetry breaking the SM Higgs field gains nonzero vacuum expectation value v and interaction (1.1) provides heavy neutral leptons and SM (or *active*) neutrinos — with the mixing mass term ($v = 246\,\text{GeV}$)

$$M^D_\alpha \equiv F_\alpha v/\sqrt{2}\,.$$

The truly neutral nature of N allows one to introduce for it a Majorana mass term, consistent with the SM gauge invariance, resulting in the HNL Lagrangian at GeV scale

$$\mathcal{L}_{\text{HNL}} = i\bar{N}\partial\!\!\!/ N + \left(M^D_\alpha \bar{\nu}_\alpha N - \frac{M_N}{2} \bar{N}^c N + \text{h.c.} \right). \tag{1.2}$$

The mass eigenstates of the active-plus-sterile sector are the mixtures of ν and N, but with small mixing angles and large splitting between mass scales of sterile and active neutrinos. The heavy mass eigenstates are "almost sterile neutrinos" while light mass eigenstates are "almost active neutrinos". In what follows we keep the same terminology for the mass states as for the gauge states. As a result of mixing, HNL couples to the SM fileds in the same way as active neutrinos,

$$\mathcal{L}_{\text{int}} = \frac{g}{2\sqrt{2}} W^+_\mu \overline{N^c} \sum_\alpha U^*_\alpha \gamma^\mu (1-\gamma_5) \ell^-_\alpha + \frac{g}{4\cos\theta_W} Z_\mu \overline{N^c} \sum_\alpha U^*_\alpha \gamma^\mu (1-\gamma_5) \nu_\alpha + \text{h.c.}\,, \tag{1.3}$$

except the coupling is strongly suppressed by the small *mixing angles*

$$U_\alpha = M^D_\alpha M_N^{-1} \tag{1.4}$$

In (1.3) ℓ_α are charged leptons of the three SM generations.

The number of model parameters increase with the number of HNLs (see e.g. reviews [3, 4]). In particular in the model with 2 sterile neutrinos there are 11 free parameters and in the case of 3 sterile neutrinos there are 18 parameters [3]. Not all of them play important role in phenomenology. The collider phenomenology is sensitive only to masses of the HNL(s) and absolute values of mixing angles, $|U_\alpha|$. When sterile neutrinos are not degenerate in mass, in all the processes they are produced and decay independently, without oscillations between themselves, in contrast to the behavior of active neutrinos [48, 58, 59]. So, from the phenomenological point of view it is enough to describe only 1 sterile neutrino, which needs only 4 parameters: sterile neutrino mass M_N and sterile neutrino mixings with all three active neutrinos U_α, eq. (1.2).

The papers is organized as follows: in section 2 we review the different HNL production channels; in section 3 we discuss the most relevant HNL decay channels. The summary and final discussion is given in the section 4. Appendices provide necessary technical clarifications.

JHEP11(2018)032

2 HNL production in proton fixed target experiments

In fixed target experiments (such as NA62, SHiP or DUNE) the initial interaction is proton-nuclei collision. In such collisions HNLs can be produced in a number of ways:

a) Production from hadron's decays;

b) Production from Deep Inelastic Scattering (DIS) p-nucleon interaction;

c) Production from the coherent proton-nucleus scattering.

Below we provide overview of each of the channels summarizing previous results and emphasizing novel points.

2.1 Production from hadrons

The main channels of HNL production from hadrons are via decays of sufficiently long-lived hadrons, i.e. the lightest hadrons of each flavour.[1] In the framework of the Fermi theory, the decays are inferred by the weak charged currents. One can also investigate the hidden flavored mesons $J/\psi(c\bar{c}, 3097)$, $\Upsilon(b\bar{b}, 9460)$ as sources of HNLs. These mesons are short-lived, but 1.5–2 times heavier than the corresponding open flavored mesons, giving a chance to produce heavier HNLs.

As the region of HNL masses below that of the kaon is strongly bounded by the previous experiments (see [5] for details, reproduced in figure 1), in what follows we concentrate on production channels for HNL masses $M_N > 0.5$ GeV.

HNLs are produced in meson decays via either 2-body purely leptonic decays (left panel of figure 2) or semileptonic decays (right panel of figure 2) [63, 64]. The branching fractions of leptonic decays have been found e.g. in [49, 51]. For the semileptonic decays only the processes with a single pseudo-scalar or vector meson in the final state have been considered so far [51] (see also [55] and [37])

$$h \to h'_P \ell N \tag{2.1}$$

$$h \to h'_V \ell N \tag{2.2}$$

(where h'_P is a *pseudo-scalar* and h'_V is a *vector* meson) and their branching ratio has been computed. We reproduce these computations in the appendix A paying special attention to the treatment of form factors.

Finally, to calculate the number of produced HNLs one should ultimately know the *production fraction*, $f(\bar{q}q \to h)$ — the probability to get a given hadron from the corresponding heavy quark. The latter can either be determined experimentally or computed from Pythia simulations (as e.g. in [57]).

2.1.1 Production from light unflavored and strange mesons

Among the light unflavored and strange mesons the relevant mesons for the HNL production are:[2] $\pi^+(u\bar{d}, 139.6)$, $K^+(u\bar{s}, 494)$, $K^0_S(d\bar{s}, 498)$ and $K^0_L(d\bar{s}, 498)$.

[1] Such hadrons decay *only* through weak interactions with relatively small decay width (as compared to electromagnetic or strong interaction). As the probability of HNL production from the hadron's decay is inversely proportional to the hadron's decay width, the HNL production from the lightest hadrons is significantly more efficient.

[2] The particle lists here and below is given in the format 'Meson name(quark contents, mass in MeV)').

JHEP11(2018)032

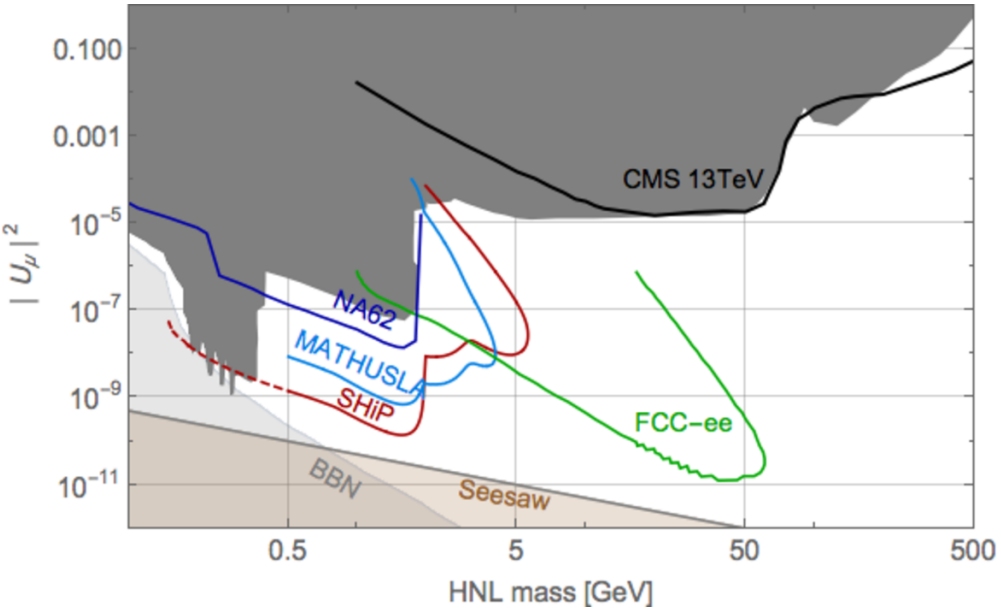

Figure 1. Existing limits and future prospects for searches for HNLs. Only mixing with muon flavour is shown. For the list of previous experiments (gray area) see [5]. Black solid line is the recent bounds from the CMS 13 TeV run [23]. The sensitivity estimates from prospective experiments are based on [27] (FCC-ee), [9] (NA62), [60] (SHiP) and [61] (MATHUSLA@LHC). The sensitivity of SHiP below kaon mass (dashed line) is based on the number of HNLs produced in the decay of D-mesons only and does not take into account contributions from kaon decays, see [60] for details. The primordial nucleosynthesis bounds on HNL lifetime are from [62]. The Seesaw line indicates the parameters obeying the seesaw relation $|U_\mu|^2 \sim m_\nu/M_N$, where for active neutrino mass we substitute $m_\nu = \sqrt{\Delta m^2_{\rm atm}} \approx 0.05\,\text{eV}$ [5].

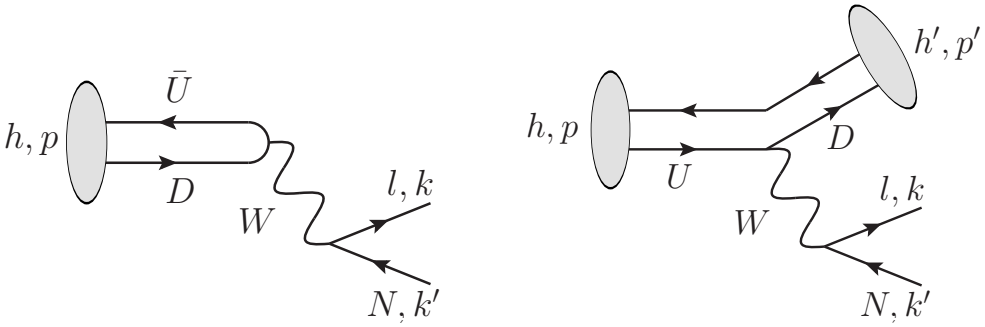

Figure 2. *Left:* the diagram of leptonic decay of the meson h with 4-momentum p. *Right:* the diagram of semileptonic decay of the meson h with 4-momentum p into meson h' with 4-momentum p'. In both diagrams the transferred to the lepton pair 4-momentum is $q = k + k'$.

The only possible production channel from the π^+ is the two body decay $\pi^+ \to \ell^+_\alpha N$ with $\ell = e, \mu$. The production from K^+ is possible through the two-body decay of the same type. There are also 3-body decays $K^+ \to \pi^0 \ell^+_\alpha N$ and $K^0_{L/S} \to \pi^- \ell^+_\alpha N$.

The resulting branching ratios for corresponding mesons are shown in figure 3. For small HNL masses the largest branching ratio is that of $K^0_L \to \pi^- \ell^+_\alpha N$ due to the helicity suppression in the two-body decays and small K^0_L decay width.

JHEP11(2018)032

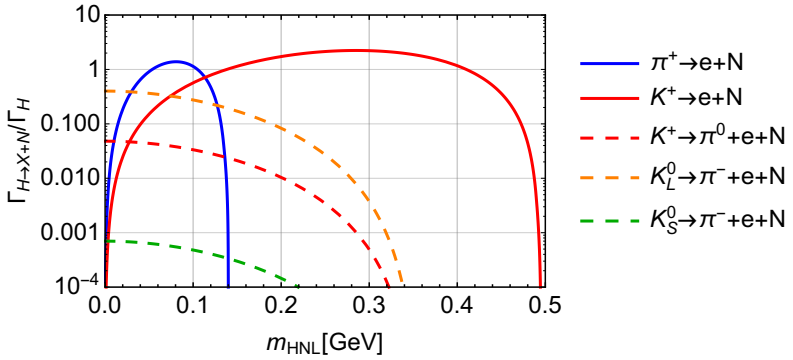

Figure 3. Light mesons decay width to HNLs related to the measured value of the total decay width for pions and kaons correspondingly. In this figure we take $U_e = 1$, $U_\mu = U_\tau = 0$. The ratio for two-body decay channels exceeds 1 due to the helicity enhancement when a massive HNL is present in the final state instead of neutrino.

2.1.2 Production from charmed mesons

The following charmed mesons are most relevant for the HNL production: $D^0(c\bar{u}, 1865)$, $D^+(c\bar{d}, 1870)$, $D_s(c\bar{s}, 1968)$.

D^0 is a neutral meson and therefore its decay through the charged current interaction necessarily involves a meson in a final state. The largest branching is to K meson, owing to the CKM suppression $|V_{cd}|/|V_{cs}| \approx 0.22$. Then the mass of the resulting HNL is limited as $M_N < M_D - M_K \approx 1.4\,\mathrm{GeV}$. For the charmed *baryons* the same argument is applicable: they should decay into baryons and the most probable is strange baryon, hence $M_N < M_{\Lambda_c} - M_\Lambda \approx 1.2\,\mathrm{GeV}$. Therefore these channels are open only for HNL mass *below* $\sim 1.4\,\mathrm{GeV}$.

Charged charmed mesons $D^\pm$ and D_s would exhibit two body decays into an HNL and a charged lepton, so they can produce HNLs almost as heavy at themselves. The branching of $D_s \to N + X$ is more than a factor 10 larger than any similar of other D-mesons. The number of D_s mesons is of course suppressed as compared to $D^\pm$ and D^0 mesons, however only by a factor of few.[3] Indeed, at energies relevant for $\bar{c}c$ production, the fraction of strange quarks is already sizeable, $\chi_{\bar{s}s} \sim 1/7$ [65]. *As a result, the two-body decays of D_s mesons dominate in the HNL production from charmed mesons*, see figure 4.

2.1.3 Production from beauty mesons

The lightest beauty mesons are $B^-(b\bar{u}, 5279)$, $B^0(b\bar{d}, 5280)$, $B_s(b\bar{s}, 5367)$, $B_c(b\bar{c}, 6276)$. Similarly to the D^0 case, neutral B-mesons (B^0 and B_s) decay through charged current with a meson in a final state. The largest branching is to D meson because of the values of CKM matrix elements ($|V_{cb}|/|V_{ub}| \approx 0.1$). Thus the mass of the resulting HNL is limited: $M_N < M_B - M_D \approx 3.4\,\mathrm{GeV}$.

Charged beauty mesons $B^\pm$ and $B_c^\pm$ have two body decays into HNL and charged lepton, so they can produce HNLs almost as heavy at themselves. Due to the CKM

[3]For example at SPS energy (400 GeV) the production fractions of the charmed mesons are given by $f(D^+) = 0.204$, $f(D^0) = 0.622$, $f(D_s) = 0.104$ [57].

JHEP11(2018)032

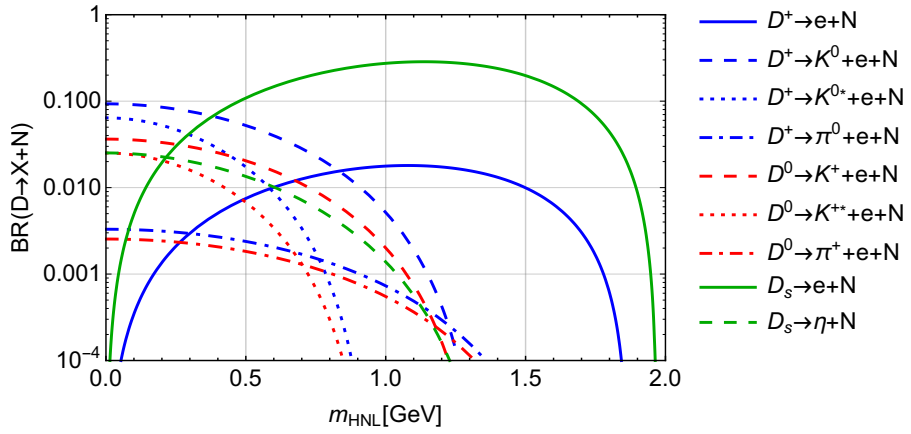

Figure 4. Dominant branching ratios of HNL production from different charmed and beauty mesons. For charged mesons two-body leptonic decays are shown, while for the neutral mesons decays are necessarily semi-leptonic. For these plots we take $U_e = 1$, $U_\mu = U_\tau = 0$.

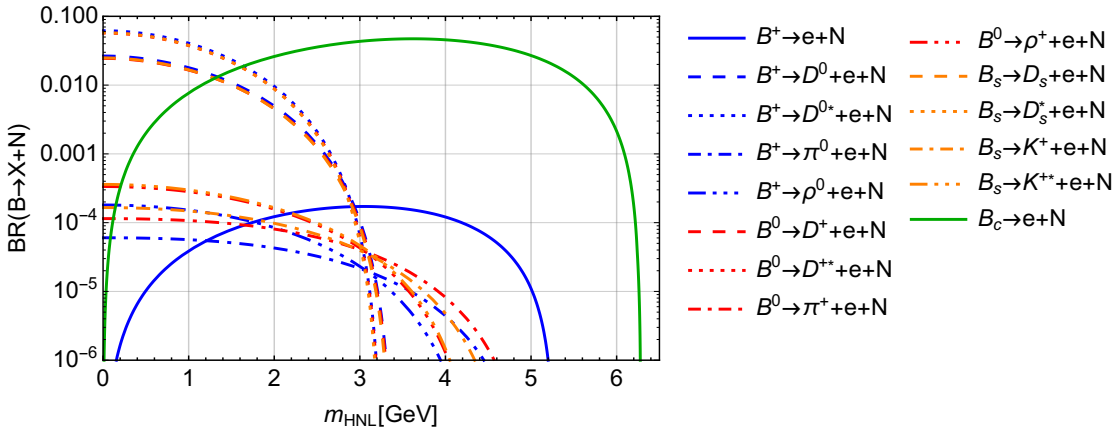

Figure 5. Dominant branching ratios of HNL production from different beauty mesons. For charged mesons two-body leptonic decays are shown, while for the neutral mesons decays are necessarily semi-leptonic. For these plots we take $U_e = 1$, $U_\mu = U_\tau = 0$.

suppression the branching ratio of $B^+ \to N + \ell^+$ is significantly smaller than that of $B_c \to N + \ell$. However, unlike the case of D_s mesons, the production fraction of $f(b \to B_c)$ has only been measured at LHC energies, where it is reaching few $\times\, 10^{-3}$ [66]. At lower energies it is not known. Branching ratio of B-mesons into HNL for different decay channels and pure electron mixing is shown at figure 5.

2.1.4 Multi-hadron final states

D and especially B mesons are heavy enough to decay into HNL and multimeson final states. While any single multi-meson channel would be clearly phase-space suppressed as compared to 2-body or 3-body decays, considered above, one should check that the "inclusive" multi-hadron decay width does not give a sizeable contribution.

JHEP11(2018)032

Decay $B^+ \to \ell^+\nu_\ell X$		BR [%]
Inclusive branching: $l = e,\, \mu$		11.0 ± 0.3
Dominant one-meson channels: pseudo-scalar meson	$\overline{D}^0\ell^+\nu_\ell$	2.27 ± 0.11
vector meson	$\overline{D}^*(2007)^0\ell^+\nu_\ell$	5.7 ± 0.19
Two above channels together:		8.0 ± 0.2
Channels with 2 meson:	$D^-\pi^+\ell^+\nu_\ell$	0.42 ± 0.05
	$D^{*-}\pi^+\ell^+\nu_\ell$	0.61 ± 0.06
$D^-\pi^+\ell^+\nu_\ell$ above is saturated by 1 meson modes	$\overline{D}_0^*(2420)^0\ell^+\nu_\ell$	0.25 ± 0.05
	$\overline{D}_2^*(2460)^0\ell^+\nu_\ell$	0.15 ± 0.02
$D^{*-}\pi^+\ell^+\nu_\ell$ is augmented with 1 meson modes	$\overline{D}_1(2420)^0\ell^+\nu_\ell$	0.30 ± 0.02
	$\overline{D}_1'(2430)^0\ell^+\nu_\ell$	0.27 ± 0.06
	$\overline{D}_2^*(2460)^0\ell^+\nu_\ell$	0.1 ± 0.02
Hence 1-meson modes contribute additionally		1.09 ± 0.12
Sum of other multimeson channels, $n > 1$:	$\overline{D}^{(*)}n\pi\ell^+\nu_\ell$	0.84 ± 0.27
Inclusive branching: $l = \tau$		not known
Dominant one-meson channels: pseudo-scalar meson	$\overline{D}^0\tau^+\nu_\tau$	0.77 ± 0.25
vector meson	$\overline{D}^*(2007)^0\tau^+\nu_\tau$	1.88 ± 0.20

Table 1. Experimentally measured branching widths for the main semileptonic decay modes of the B^+ and B^0 meson [65]. Decays to pseudoscalar (D) and vector (D^*) mesons together constitute 73% (for B^+) and 69% (for B^0). Charmless channels are not shown because of their low contribution.

To estimate relative relevance of single and multi-meson decay channels, we first consider the branching ratios of the semileptonic decays of B^+ and B^0 (with ordinary (massless) neutrino ν_ℓ in the final state)

$$B \to \ell^+\nu_\ell X \quad , \quad l = e,\, \mu\,, \tag{2.3}$$

where X are one or many hadrons. The results are summarized in table 1. Clearly, by taking into account *only* single meson states we would *underestimate* the total inclusive width of the process (2.3) by about 20%.

In case of semileptonic decays in the HNL in the final state, the available phase space shrinks considereably, see figure 6. The effect of the mass can also be estimated by comparing the decays involving light leptons (e/μ) and τ-lepton in the final state. A comparison with SM decay rates into τ-lepton shows that 3-body decays into heavy sterile neutrinos are suppressed with respect to decays to light neutrinos. *Thus inclusive semi-leptonic decay of flavoured mesons to HNLs are dominated by single-meson final states with the contributions from other state introducing small correction.*

JHEP11(2018)032

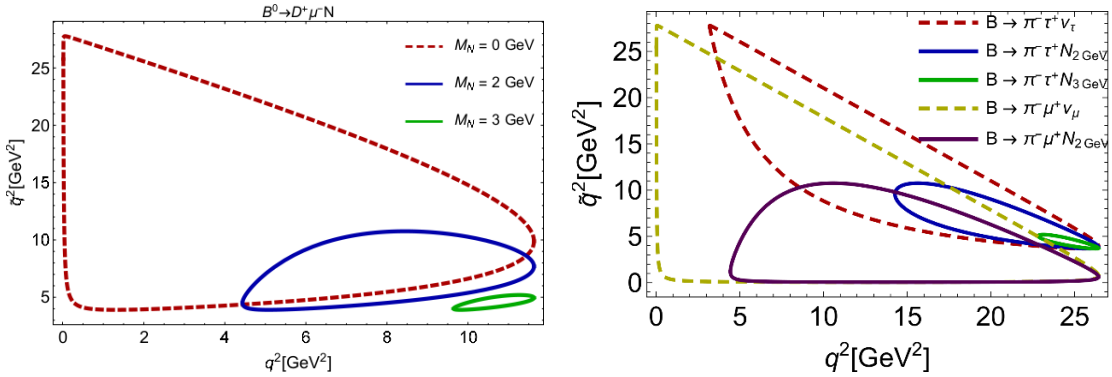

Figure 6. Dalitz plot for the semileptonic decay $B^0 \to D^+\mu^- N$. Available phase-space shrinks drastically when HNL mass is large. q^2 is the invariant mass of the lepton pair, $\tilde{q}^2$ is the invariant mass of the final meson and charged lepton.

2.1.5 Quarkonia decays

Next we investigate the hidden flavored mesons $J/\psi(c\bar{c}, 3097)$ and $\Upsilon(b\bar{b}, 9460)$ as sources of HNLs. These mesons are short-lived, but 1.5–2 times heavier than the corresponding open flavored mesons, giving a chance to produce heavier HNLs. We have studied these mesons in appendix D, here we provide the summary of the results.

The number of HNLs produced from J/ψ decays is always subdominant to the number of HNLs produced in D-meson decays (for $M_N < m_D$). Therefore, the range of interest is $2\,\text{GeV} \leq M_N \leq m_{J/\psi}$ where this number should be compared with the number of HNLs produced via B-meson decays. The resulting ratio is given by

$$\frac{\text{HNLs from } J/\psi}{\text{HNLs from } B} = \frac{X_{c\bar{c}} \times f(J/\psi) \times \text{BR}_{J/\psi \to N\bar{\nu}}}{X_{b\bar{b}} \times f(B) \times \text{BR}_{B \to NX}} = 3 \times 10^{-4} \left(\frac{X_{c\bar{c}}}{10^{-3}}\right) \left(\frac{10^{-7}}{X_{b\bar{b}}}\right) \tag{2.4}$$

where $X_{q\bar{q}}$ is the $q\bar{q}$ production rate and $f(h)$ is a production fraction for the given meson (see values for the SHiP experiment in appendix E). We have adopted $f(B) \times \text{BR}(B \to N + X) \sim 10^{-2}$ (cf. figure 5) and used $f(J/\psi) \sim 10^{-2}$. The numbers in (2.4) are normalized to the 400 GeV SPS proton beam. One sees that J/ψ can play a role only below $b\bar{b}$ production threshold (as $X_{b\bar{b}}$ tends to zero).

For experiments where sizeable number of $b\bar{b}$ pairs is produced one can use the Υ decays to produce HNLs with $M_N \gtrsim 5\,\text{GeV}$. The number of thus produced HNLs is given by

$$N_{\Upsilon \to N\bar{\nu}} \simeq 10^{-10} N_\Upsilon \times \left(\frac{U^2}{10^{-5}}\right) \tag{2.5}$$

where N_Υ is the total number of Υ mesons produced and we have normalized U^2 to the current experimental limit for $M_N > 5\,\text{GeV}$ (cf. figure 1). It should be noted that HNLs with the mass of 5 GeV and $U^2 \sim 10^{-5}$ have the decay length $c\tau \sim$ cm.

2.1.6 Production from baryons

Semileptonic decays of heavy flavoured baryons (table 2) produce HNLs. Baryon number conservation implies that either proton or neutron (or other heavier baryons) must be

JHEP11(2018)032

Strange baryons	$\Lambda^0(uds, 1116)$, $\Sigma^+(uus, 1189)$, $\Sigma^-(dds, 1197)$, $\Xi^0(uss, 1315)$, $\Xi^-(dss, 1322)$, $\Omega^-(sss, 1672)$
Charmed baryons	$\Lambda_c(udc, 2287)$, $\Sigma_c^{++}(uuc, 2453)$, $\Sigma_c^0(ddc, 2453)$, $\Xi_c^+(usc, 2468)$, $\Xi_c^0(dsc, 2480)$, $\Omega_c^-(ssc, 2695)$, $\Xi_{cc}^+(dcc, 3519)$
Beauty baryons	$\Lambda_b(udb, 5619)$, $\Sigma_b^+(uub, 5811)$, $\Sigma_b^-(ddb, 5815)$, $\Xi_b^0(usb, 5792)$, $\Xi_b^-(dsb, 5795)$, $\Omega_b^-(ssb, 6071)$

Table 2. Long-lived flavoured baryons. For each quark content (indicated in parentheses) only the lightest baryon of a given quark contents (ground state, masses are in MeV) is shown, see footnote 1. Baryons considered in [57] have blue background. Unobserved so far baryons (such as $\Omega_{cc}^+(scc)$, $\Omega_{cb}(scb)$, etc.) are not listed.

produced in the heavy baryon decay, which shrink by about 1 GeV the kinematical window for sterile neutrino. The corresponding heavy meson decays have an obvious advantage in this respect. Moreover, since both baryons and sterile neutrinos are fermions, only the baryon decays into three and more particles in the final state can yield sterile neutrinos, which further shrinks the sterile neutrino kinematical window with respect to the meson case, where two-body, pure leptonic decays can produce sterile neutrinos.

Furthermore, light flavored baryons, strange baryons (see table 2) can only produce HNLs in the mass range where the bounds are very strong already (roughly below kaon mass, see figure 1). Indeed, as weak decays change the strangeness by 1 unit, there the double-strange Ξ-baryons can only decay to Λ or Σ baryons (plus electron or muon and HNL). The maximal mass of the HNL that can be produced in this process is *smaller* than $(M_{\Xi^-} - M_{\Lambda^0}) \simeq 200\,\text{MeV}$. Then, Ω^- baryon decays to $\Xi^0\ell^-N$ with the maximal HNL mass not exceeding $M_{\Omega^-} - M_{\Xi^0} \simeq 350\,\text{MeV}$. Finally, weak decays of Λ or Σ baryons to (p, n) can produce only HNLs lighter than $\sim 250\,\text{MeV}$.

The production of HNL in the decays of charmed and beauty hyperons has been investigated in ref. [52], which results have been recently checked in [67]. The number of such baryons is of course strongly suppressed as compared to the number of mesons with the same flavour. At the same time the masses of HNLs produced in the decay of charmed (beauty) baryons are *below* the threshold of HNL production of the corresponding charm (beauty) mesons due to the presence of a baryon in the final state. This makes such a production channel strongly subdominant. A dedicated studies for SHiP [57] and at the LHC [67] confirm this conclusion. It should be noted that refs. [52, 57] use form factors from ref. [68] which are about 20 years old. A lot of progress has been made since then (see e.g. [69, 70], where some of these form factors were re-estimated and a factor ~ 2 difference with the older estimates were established).

2.2 HNL production from tau lepton

At centre of mass energies well above the $\bar{c}c$ threshold τ-leptons are copiously produced mostly via $D_s \to \tau + X$ decays. Then HNLs can be produced in τ decay and these decays are important in the case of dominant mixing with τ flavour (which is the least constrained, see [5, Chapter 4]). The main decay channels of τ are $\tau \to N + h_{P/V}$, $\tau \to N\ell_\alpha\bar{\nu}_\alpha$ and

JHEP11(2018)032

$\tau \to \nu_\tau \ell_\alpha N$, where $\alpha = e, \mu$. The computations of the corresponding decays widths are similar to the processes $N \to \ell_\alpha h_{P/V}$ (cf. appendix B.2) and purely leptonic decays of HNL (see section 3.1.1). The results are

$$\Gamma(\tau \to N h_P) = \frac{G_F^2 f_h^2 m_\tau^3}{16\pi} |V_{UD}|^2 |U_\tau|^2 \left[\left(1 - y_N^2\right)^2 - y_h^2 (1 + y_N^2) \right] \sqrt{\lambda(1, y_N^2, y_h^2)} \tag{2.6}$$

$$\Gamma(\tau \to N h_V) = \frac{G_F^2 g_h^2 m_\tau^3}{16\pi m_h^2} |V_{UD}|^2 |U_\tau|^2 \left[\left(1 - y_N^2\right)^2 + y_h^2 (1 + y_N^2 - 2y_h^2) \right] \sqrt{\lambda(1, y_N^2, y_h^2)} \tag{2.7}$$

$$\begin{aligned} \Gamma(\tau \to N \ell_\alpha \bar{\nu}_\alpha) &= \frac{G_F^2 m_\tau^5}{96\pi^3} |U_\tau|^2 \int_{y_\ell^2}^{(1-y_N)^2} \frac{d\xi}{\xi^3} \left(\xi - y_\ell^2\right)^2 \sqrt{\lambda(1, \xi, y_N^2)} \\ &\quad \times \left(\left(\xi + 2y_\ell^2\right) \left[1 - y_N^2\right]^2 + \xi \left(\xi - y_\ell^2\right) \left[1 + y_N^2 - y_\ell^2\right] - \xi y_\ell^4 - 2\xi^3 \right) \\ &\approx \frac{G_F^2 m_\tau^5}{192\pi^3} |U_\tau|^2 \left[1 - 8y_N^2 + 8y_N^6 - y_N^8 - 12 y_N^4 \log(y_N^2)\right], \quad \text{for } y_l \to 0 \end{aligned} \tag{2.8}$$

$$\begin{aligned} \Gamma(\tau \to \nu_\tau \ell_\alpha N) &= \frac{G_F^2 m_\tau^5}{96\pi^3} |U_\alpha|^2 \int_{(y_\ell + y_N)^2}^{1} \frac{d\xi}{\xi^3} (1 - \xi)^2 \sqrt{\lambda(\xi, y_N^2, y_\ell^2)} \\ &\quad \times \left(2\xi^3 + \xi - \xi(1 - \xi) \left[1 - y_N^2 - y_\ell^2\right] - (2 + \xi) \left[y_N^2 - y_\ell^2\right]^2 \right) \\ &\approx \frac{G_F^2 m_\tau^5}{192\pi^3} |U_\alpha|^2 \left[1 - 8y_N^2 + 8y_N^6 - y_N^8 - 12 y_N^4 \log(y_N^2)\right], \quad \text{for } y_l \to 0 \end{aligned} \tag{2.9}$$

where $y_i = m_i / m_\tau$, V_{UD} is an element of CKM matrix which corresponds to quark content of the meson h_P, f_h and g_h are pseudoscalar and vector meson decay constants (see tables 8 and 9) and λ is the Källén function [71]:

$$\lambda(a, b, c) = a^2 + b^2 + c^2 - 2ab - 2ac - 2bc \tag{2.10}$$

The results of this section fully agree with literature [51].

2.3 HNL production via Drell-Yan and other parton-parton scatterings

The different matrix elements for HNL production in proton-proton collision are shown in figure 7. Here we are limited by the beam energy not high enough to produce real weak bosons on the target protons. There are three type of processes: Drell-Yan-type process a), gluon fusion b) and $W\gamma/g$ fusion c). Process b) starts to play an important role for much higher centre-of-mass energies [72, 73], process a) and c) should be studied more accurately.

Let us start with the process a) in figure 7. The cross section at the parton level is [74, 75]

$$\sigma(\bar{q} q' \to N \ell) = \frac{G_F^2 |V_{qq'}|^2 |U_\ell|^2 s_{\bar{q}q'}}{6 N_c \pi} \left(1 - \frac{3M_N^2}{2s_{\bar{q}q'}} + \frac{M_N^6}{2s_{\bar{q}q'}^3}\right), \quad s_{\bar{q}q'} > M_N^2 \tag{2.11}$$

where $V_{qq'}$ is an element of the CKM matrix, $N_c = 3$ is a number of colors and the centre-of-mass energy of the system $\bar{q}q'$ is given by

$$s_{\bar{q}q'} = s x_1 x_2 \tag{2.12}$$

JHEP11(2018)032

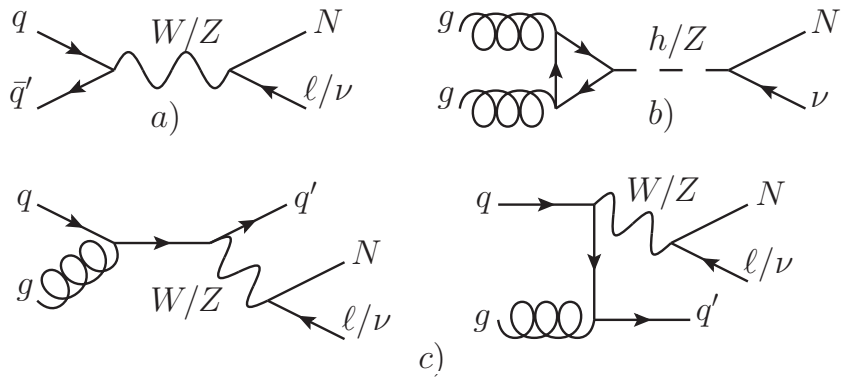

Figure 7. HNL production channels: a) Drell-Yan-type process; b) gluon fusion; c) quark-gluon fusion.

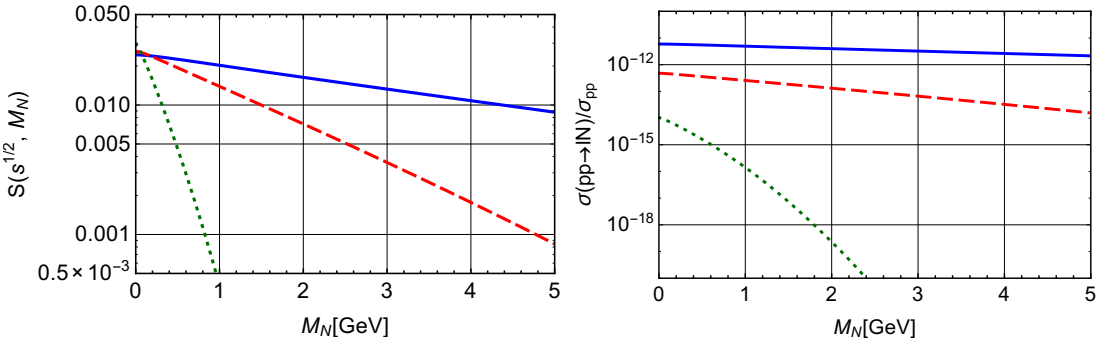

Figure 8. Integral (2.13) as a function of HNLs mass, neglecting lepton mass (left panel) and Probability of HNL production in p-p collision for $|U_\ell| = 1$ (right panel) for $\sqrt{s} = 100\,\text{GeV}$ (blue line), $\sqrt{s} = 28\,\text{GeV}$ (red dashed line) and $\sqrt{s} = 4\,\text{GeV}$ (green dotted line). The suppression of the integral as compared to $M_N = 0$ case is due to PDFs being small at $x \sim 1$ and condition $x_1 x_2 s > M_N^2$. Total p-p cross section is taken from [65].

where x_1 and x_2 are fractions of the total proton's momentum carried by the quark q' and anti-quark $\bar{q}$ respectively. The total cross section therefore is written as

$$\begin{aligned}\sigma(\bar{q}q' \to N\ell) &= 2\sum_{\bar{q},q'} \frac{G_F^2 |V_{qq'}|^2 |U_\ell|^2 s}{6N_c\pi} \\ &\times \int \frac{dx_1}{x_1}\, x_1^2 f_{\bar{q}}(x_1, s_{\bar{q}q'}) \int \frac{dx_2}{x_2}\, x_2^2 f_{q'}(x_2, s_{\bar{q}q'}) \left(1 - \frac{3M_N^2}{2sx_1x_2} + \frac{M_N^6}{2s^3 x_1^3 x_2^3}\right) \\ &\equiv \frac{G_F^2 |V_{qq'}|^2 |U_\ell|^2 s}{6N_c\pi}\, S(\sqrt{s}, M_N) \end{aligned} \tag{2.13}$$

where $f_q(x, Q^2)$ is parton distribution function (PDF). The corresponding integral $S(\sqrt{s}, M_N)$ as a function of M_N and the production probability for this channel are shown in figure 8. For numerical estimates we have used LHAPDF package [76] with CT10NLO pdf set [77].

This can be roughly understood as follows: PDFs peak at $x \ll 1$ (see figure 9) and therefore the probability that the center-of-mass energy of a parton pair exceeds the HNL

JHEP11(2018)032

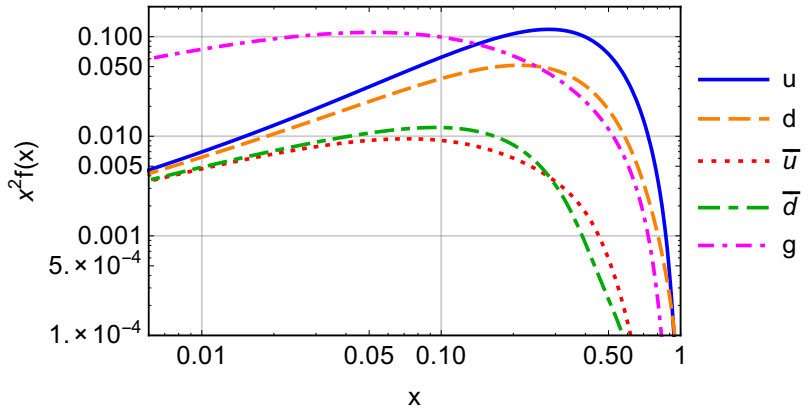

Figure 9. Combination $x^2 f(x)$ used in eq. (2.13) for quark and gluon PDFs (for $\sqrt{s} \sim 30\,\text{GeV}$). The functions peak at small values of x and therefore a probability of the centre-of-mass energy of the parton pair close to $\sqrt{s}$ is small.

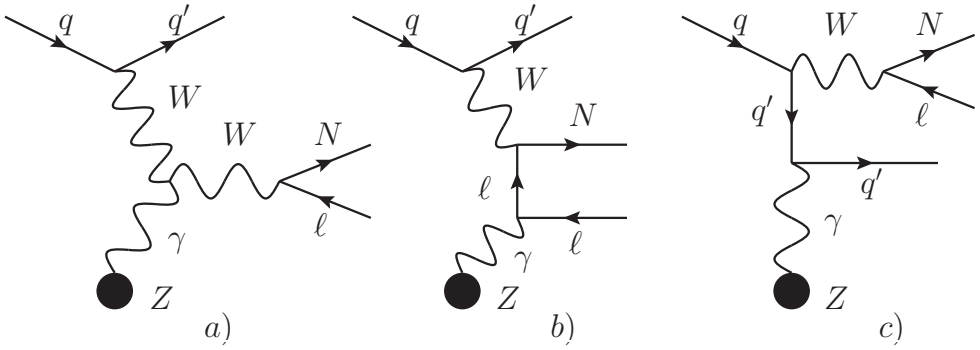

Figure 10. Possible Feynman diagrams for the HNL production in the proton coherent scattering off the nuclei.

mass, $\sqrt{s_{\text{parton}}} \gg M_N$, is small. On the other hand, the probability of a flavour meson to decay to HNL (for $|U|^2 \sim 1$) is of the order of few % and therefore "wins" over the direct production, especially at the fixed-target experiments where beam energies do not exceed hundreds of GeV. In case of the quark-gluon initial state (process c) in figure 7) the similar considerations also work and the resulting cross section is also small, with an additional suppression due to the 3-body final state. *We see that the direct production channel is strongly suppressed in comparison with the production from mesons for HNLs with masses* $M_N \lesssim 5\,\text{GeV}$.

2.4 Coherent proton-nucleus scattering

The coherent scattering of a proton off the nuclei as a whole could be an effective way of producing new particles in fixed target experiments. There are two reasons for this. First, parton scattering in the electromagnetic field of the nuclei is proportional to Z^2 (where Z is the nuclei charge) which can reach a factor 10^3 enhancement for heavy nuclei. Second, the centre of mass energy of proton-nucleus system is higher than for the proton-proton scattering. The coherent production of the HNLs will be discussed in the forthcoming

JHEP11(2018)032

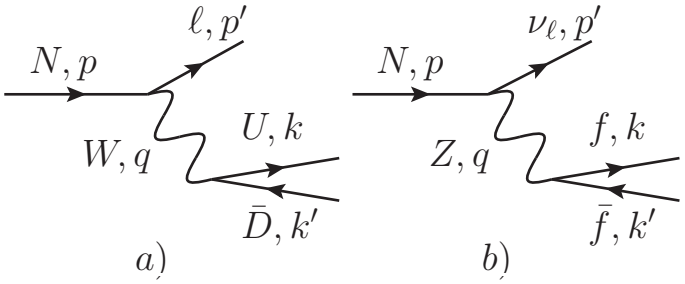

Figure 11. Diagram for the HNL decays mediated by charged a) and neutral b) currents.

paper [78]. Here we announce the main result: the HNL coherent production channel is subdominant to the meson decay for all HNL masses and mixing angles (for HNL masses below 5 GeV). In case of SHiP on expects less than 1 HNL *produced* via coherent scattering for 10^{20} PoT.

2.5 Summary

In summary, production of HNL in proton fixed target experiments occurs predominantly via (semi)leptonic decays of the lightest c- and b- mesons (figures 4, 5). The production from heavier mesons is suppressed by the strong force mediated SM decays, while production from baryons is kinematically suppressed. Other production channels are subdominant for all masses $0.5\,\text{GeV} \leq M_N \leq 5\,\text{GeV}$ as discussed in sections 2.3–2.4.

3 HNL decay modes

All HNL decays are mediated by charged current or neutral current interactions (1.3). In this section we systematically revisit the most relevant decay channels. Most of the results for sufficiently light HNLs exist in the literature [37, 49–51, 53, 54]. For a few modes there are discrepancies by factors of few between different works, we comment on these discrepancies in due course.

All the results presented below *do not take into account charge conjugated channels* which are possible for the Majorana HNL; to account for the Majorana nature one should multiply by 2 all the decay widths. The branching ratios are the same for Majorana case and for the case considered here.

3.1 3-body basic channels

Two basic diagrams, presented in the figure 11, contribute to all decays. For the charged current-mediated decay (figure 11(a)) the final particles (U, D) could be either a lepton pair $(\nu_\alpha, \ell_\alpha)$ or a pair of up and down quarks (u_i, d_j). For the neutral current-mediated decay f is any fermion. The tree-level decay width into free quarks, while unphysical by itself for the interesting mass range, is important in estimates of the full hadronic width at $M_N \gg \Lambda_{\text{QCD}}$, see section 3.2.2 below.

For the decays $N \to \nu_\alpha \ell_\alpha^- \ell_\alpha^+$ and $N \to \nu_\alpha \nu_\alpha \bar{\nu}_\alpha$ both diagrams contribute, which leads to the interference (see section 3.1.2).

JHEP11(2018)032

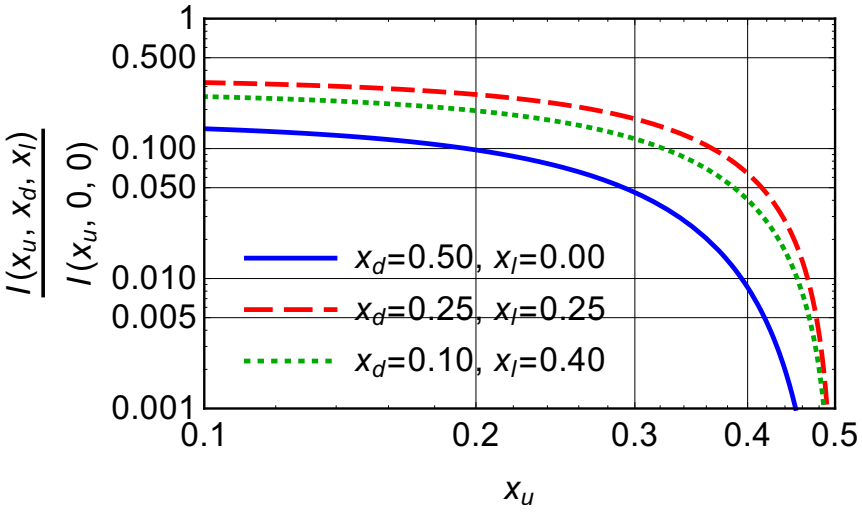

Figure 12. Function $I(x_u, x_d, x_l)/I(x_u, 0, 0)$ for several choices of x_d and x_l (see eq. (3.2) for $I(x_u, x_d, x_l)$ definition).

3.1.1 Charged current-mediated decays

The general formula for the charged current-mediated processes $N \to \ell_\alpha^- \nu_\beta \ell_\beta^+$, $\alpha \neq \beta$, and $N \to \ell_\alpha u_i \bar{d}_j$ is [50, 53, 54, 79]

$$\Gamma(N \to \ell_\alpha^- U \bar{D}) = N_W \frac{G_F^2 M_N^5}{192\pi^3} |U_\alpha|^2 I(x_u, x_d, x_l) \tag{3.1}$$

where $x_l = \dfrac{m_{\ell_\alpha}}{M_N}$, $x_u = \dfrac{m_U}{M_N}$, $x_d = \dfrac{m_D}{M_N}$. The factor $N_W = 1$ for the case of the final leptons and $N_W = N_c |V_{ij}|^2$ in the case of the final quarks, where $N_c = 3$ is the number of colors, and V_{ij} is the corresponding matrix element of the CKM matrix. The function $I(x_u, x_d, x_l)$ that describes corrections due to finite masses of final-state fermions is given by

$$I(x_u, x_d, x_l) \equiv 12 \int_{(x_d+x_l)^2}^{(1-x_u)^2} \frac{dx}{x} \left(x - x_l^2 - x_d^2\right) \left(1 + x_u^2 - x\right) \sqrt{\lambda(x, x_l^2, x_d^2)\lambda(1, x, x_u^2)}, \tag{3.2}$$

where $\lambda(a, b, c)$ is given by eq. (2.10).

Several properties of the function (3.2) are in order:

1. $I(0, 0, 0) = 1$
2. Function $I(a, b, c)$ is symmetric under *any* permutation of its arguments a, b, c.[4]
3. In the case of mass hierarchy $m_a, m_b \ll m_c$ (where a, b, c are leptons and/or quarks in some order) one can use approximate result
$$I(x, 0, 0) = (1 - 8x^2 + 8x^6 - x^8 - 12x^4 \log x^2) \tag{3.3}$$
where $x = \dfrac{m_c}{M_N}$
4. The ratio $I(x_u, x_d, x_l)/I(x_u, 0, 0)$ for several choices of x_d, x_l is plotted in figure 12. It decreases with each argument.

[4]This property is non-obvious but can be verified by the direct computation.

JHEP11(2018)032

f	C_1^f	C_2^f
$u,\, c,\, t$	$\frac{1}{4}\left(1-\frac{8}{3}\sin^2\theta_W+\frac{32}{9}\sin^4\theta_W\right)$	$\frac{1}{3}\sin^2\theta_W\left(\frac{4}{3}\sin^2\theta_W-1\right)$
$d,\, s,\, b$	$\frac{1}{4}\left(1-\frac{4}{3}\sin^2\theta_W+\frac{8}{9}\sin^4\theta_W\right)$	$\frac{1}{6}\sin^2\theta_W\left(\frac{2}{3}\sin^2\theta_W-1\right)$
$\ell_\beta,\, \beta\neq\alpha$	$\frac{1}{4}\left(1-4\sin^2\theta_W+8\sin^4\theta_W\right)$	$\frac{1}{2}\sin^2\theta_W\left(2\sin^2\theta_W-1\right)$
$\ell_\beta,\, \beta=\alpha$	$\frac{1}{4}\left(1+4\sin^2\theta_W+8\sin^4\theta_W\right)$	$\frac{1}{2}\sin^2\theta_W\left(2\sin^2\theta_W+1\right)$

Table 3. Coefficients C_1 and C_2 for the neutral current-mediated decay width.

3.1.2 Decays mediated by neutral current interaction and the interference case

Decay width for neutral current-mediated decay $N\to\nu_\alpha f\bar{f}$ depends on the type of the final fermion. For charged lepton pair $l_\beta\bar{l}_\beta$ the results are different for the case $\alpha\neq\beta$ and $\alpha=\beta$, because of the existence of the charge current mediated diagrams in the latter case. Nevertheless, the decay width can be written in the unified way,

$$\Gamma(N\to\nu_\alpha f\bar{f})=N_Z\frac{G_F^2M_N^5}{192\pi^3}\cdot|U_\alpha|^2\cdot\left[C_1^f\left((1-14x^2-2x^4-12x^6)\sqrt{1-4x^2}\right.\right.$$
$$\left.+12x^4(x^4-1)L(x)\right)+4C_2^f\left(x^2(2+10x^2-12x^4)\sqrt{1-4x^2}$$
$$\left.\left.+6x^4(1-2x^2+2x^4)L(x)\right)\right],\tag{3.4}$$

where $x=\dfrac{m_f}{M_N}$, $L(x)=\log\left[\dfrac{1-3x^2-(1-x^2)\sqrt{1-4x^2}}{x^2(1+\sqrt{1-4x^2})}\right]$ and $N_Z=1$ for the case of leptons in the final state or $N_Z=N_c$ for the case of quarks. The values of C_1^f and C_2^f are given in the table 3. This result agrees with [51, 53, 54].

In the case of pure neutrino final state only neutral currents contribute and the decays width reads

$$\Gamma(N\to\nu_\alpha\nu_\beta\bar{\nu}_\beta)=(1+\delta_{\alpha\beta})\frac{G_F^2M_N^5}{768\pi^3}|U_\alpha|^2.\tag{3.5}$$

3.2 Decay into hadrons

In this section we consider hadronic final states for M_N both below and above $\Lambda_{\rm QCD}$ scale and discuss the range of validity of our results.

3.2.1 Single meson in the final state

At $M_N\lesssim\Lambda_{\rm QCD}$ the quark pair predominantly binds into a single meson. There are charged current- and neutral current-mediated processes with a meson in the final state: $N\to\ell_\alpha h^+_{P/V}$ and $N\to\nu_\alpha h^0_{P/V}$, where h^+_P (h^0_P) are charged (neutral) pseudoscalar mesons and h^+_V (h^0_V) are charged (neutral) vector mesons. In formulas below $x_h\equiv m_h/M_N$, $x_\ell=m_\ell/M_N$, f_h and g_h are the corresponding meson decay constants (see appendix C.1),

JHEP11(2018)032

θ_W is a Weinberg angle and the function λ is given by eq. (2.10). The details of the calculations are given in the appendix B.2.

The decay width to the charged pseudo-scalar mesons $(\pi^\pm, K^\pm, D^\pm, D_s, B^\pm, B_c)$ is given by

$$\Gamma(N \to \ell_\alpha^- h_P^+) = \frac{G_F^2 f_h^2 |V_{UD}|^2 |U_\alpha|^2 M_N^3}{16\pi} \left[\left(1 - x_\ell^2\right)^2 - x_h^2 (1 + x_\ell^2) \right] \sqrt{\lambda(1, x_h^2, x_\ell^2)}, \tag{3.6}$$

in full agreement with the literature [51, 53, 54].

The decay width to the pseudo-scalar neutral meson $(\pi^0, \eta, \eta', \eta_c)$ is given by

$$\Gamma(N \to \nu_\alpha h_P^0) = \frac{G_F^2 f_h^2 M_N^3}{32\pi} |U_\alpha|^2 \left(1 - x_h^2\right)^2 \tag{3.7}$$

Our answer agrees with [51], but is twice larger than [53, 54]. The source of the difference is unknown.[5]

The HNL decay width into charged vector mesons ($\rho^\pm$, $a_1^\pm$, $D^{\pm *}$, $D_s^{\pm *}$) is given by

$$\Gamma(N \to \ell_\alpha^- h_V^+) = \frac{G_F^2 g_h^2 |V_{UD}|^2 |U_\alpha|^2 M_N^3}{16\pi m_h^2} \left(\left(1 - x_\ell^2\right)^2 + x_h^2 \left(1 + x_\ell^2\right) - 2x_h^4 \right) \sqrt{\lambda(1, x_h^2, x_\ell^2)} \tag{3.8}$$

that agrees with the literature [51, 53, 54].

However, there is a disagreement regarding the numerical value of the meson constant g_ρ between [51] and [53, 54]. We extract the value of this constant from the decay $\tau \to \nu_\tau \rho$ and obtain the result that numerically agrees with the latter works, see discussion in appendix C.1.3.

For the decay into neutral vector meson (ρ^0, a_1^0, ω, ϕ, J/ψ) we found that the result depends on the quark content of meson. To take it into account we introduce dimensionless κ_h factor to the meson decay constant (B.36). The decay width is given by

$$\Gamma(N \to \nu_\alpha h_V^0) = \frac{G_F^2 \kappa_h^2 g_h^2 |U_\alpha|^2 M_N^3}{32\pi m_h^2} \left(1 + 2x_h^2\right) \left(1 - x_h^2\right)^2 . \tag{3.9}$$

Our result for ρ^0 and results in [51] and [53] are all different. The source of the difference is unknown. For decays into ω, ϕ and J/ψ mesons we agree with [53]. The result for the a_1^0 meson appears for the first time.[6]

The branching ratios for the one-meson and lepton channels below 1 GeV are given on the left panel of figure 13.

[5] This cannot be due to the Majorana or Dirac nature of HNL, because the same discrepancy would then appear in eq. (3.6).

[6] Refs. [53, 54] quote also two-body decays $N \to \nu_\alpha h_V^0$, $h_V^0 = K^{*0}, \bar{K}^{*0}, D^{*0}, \bar{D}^{*0}$, with the rate given by (3.9) (with a different κ). This is not justified, since the weak neutral current does not couple to the corresponding vector meson h_V^0 at tree level.

JHEP11(2018)032

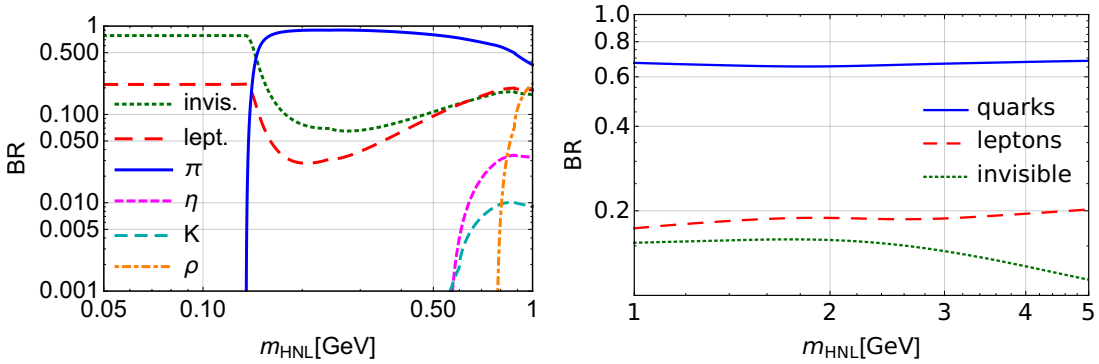

Figure 13. The branching ratios of the HNL for the mixing ratio $U_e : U_\mu : U_\tau = 1 : 1 : 1$. *Left panel:* region of masses below 1 GeV; *Right panel:* region of masses above 1 GeV, for quarks the QCD corrections (3.10), (3.11) are taken into account.

3.2.2 Full hadronic width vs. decay into single meson final state

Decays into multi-hadron final states become kinematically accessible as soon as $M_N > 2m_\pi$. To estimate their branching fractions and their contribution to the total decay width, we can compute the total hadronic decay width of HNLs, $\Gamma_{\rm had}$ and compare it with the combined width of all single-meson states, $\Gamma_{1\,\rm meson}$. The total hadronic decay width can be estimated via decay width into quarks (sections 3.1.1–3.1.2) times the additional loop corrections.

The QCD loop corrections to the tree-level decay into quarks have been estimated in case of τ lepton hadronic decays. In this case the tree level computation of the τ decay to two quarks plus neutrino underestimates the full hadronic decay width by 20% [80–82]. The loop corrections, $\Delta_{\rm QCD}$, defined via

$$1 + \Delta_{\rm QCD} \equiv \frac{\Gamma(\tau \to \nu_\tau + \text{hadrons})}{\Gamma_{\rm tree}(\tau \to \nu_\tau \bar{u} q)} \tag{3.10}$$

have been computed up to three loops [82] and is given by:

$$\Delta_{\rm QCD} = \frac{\alpha_s}{\pi} + 5.2\frac{\alpha_s^2}{\pi^2} + 26.4\frac{\alpha_s^3}{\pi^3}, \tag{3.11}$$

where $\alpha_s = \alpha_s(m_\tau)$.[7] We use (3.11) with $\alpha_s = \alpha_s(M_N)$ as an estimation for the QCD correction for the HNL decay, for both charged and neutral current processes. We expect therefore that QCD correction to the HNL decay width into quarks is smaller than 30% for $M_N \gtrsim 1$ GeV (figure 14).

Full hadronic decay width dominates the HNL lifetime for masses $M_N \gtrsim 1$ GeV (see figure 13). The latter is important to define the upper bound of sensitivity for the experiments like SHiP or MATHUSLA (see figure 1). This upper bound is defined by the requirements that HNLs can reach the detector.

[7] Numerically this gives for τ-lepton $\Delta_{\rm QCD} \approx 0.18$, which is within a few *per cent* of the experimental value $\Delta_{\rm Exp} = 0.21$. The extra difference comes from the QED corrections.

JHEP11(2018)032

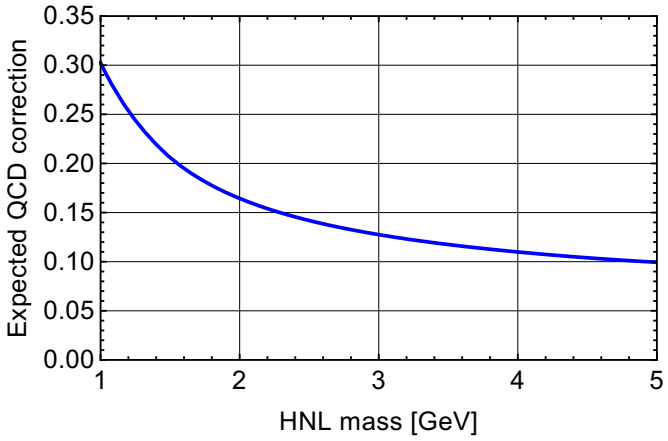

Figure 14. The estimate of the QCD corrections for the HNL decay into quark pairs, using the three-loop formula (3.11) for τ-lepton.

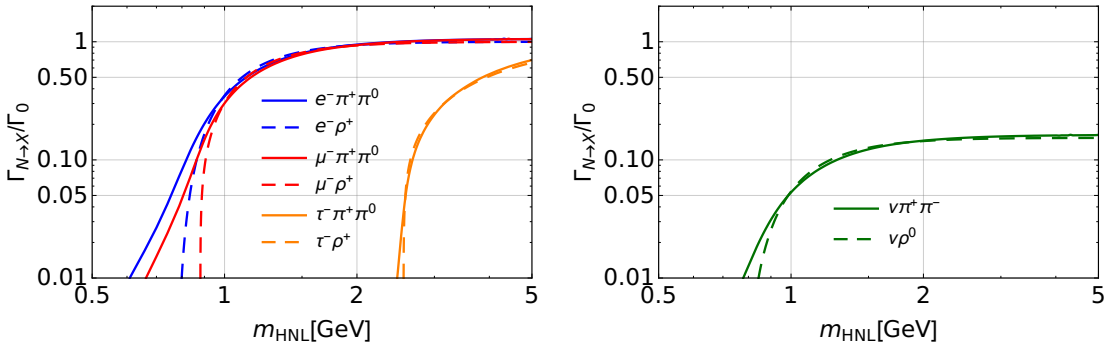

Figure 15. *Left panel:* decay widths of charged current channels with ρ or 2π divided by $\Gamma_0 = \frac{1}{16\pi} G_F^2 \frac{g_\rho^2}{m_\rho^2} |V_{ud}|^2 |U_\alpha|^2 M_N^3$, which is prefactor in eq. (3.8). *Right panel:* the same for neutral current channels.

3.2.3 Multi-meson final states

When discussing "single-meson channels" above, we have also included there decays with the ρ-meson. By doing so, we have essentially incorporated all the two-pion decays $N \to \pi^+\pi^0\ell^-$ for $M_N > m_\rho$. Indeed, we have verified by direct computation of $N \to \pi^+\pi^0\ell^-$ that they coincide with $N \to \rho^+\ell^-$ for all relevant masses (figure 15). Of course the decay channel to two pions is also open for $2m_\pi < M_N < m_\rho$, but its contribution there is completely negligible and we ignore this in what follows.

Figures 13 and 16 demonstrate that one-meson channels are definitely enough for all the hadronic modes if sterile neutrino mass does not exceed 1 GeV. The ratio between the combined decay width into single-meson final states ($\pi^\pm$, π^0, η, η', $\rho^\pm$, ρ^0, ω+ϕ, D_s) and into quarks is shown in figure 16.[8] One sees that the decay width into quarks is larger for $M_N \gtrsim 2\,\text{GeV}$, which means that multi-meson final states are important in this region.

The main expected 3- and 4-body decays channels of HNL and decay are presented in table 4. In this table we also add information about multimeson decays of τ because they

[8] We ignore CKM-suppressed decays into kaons as well as decays to heavy flavour meson (D,B).

JHEP11(2018)032

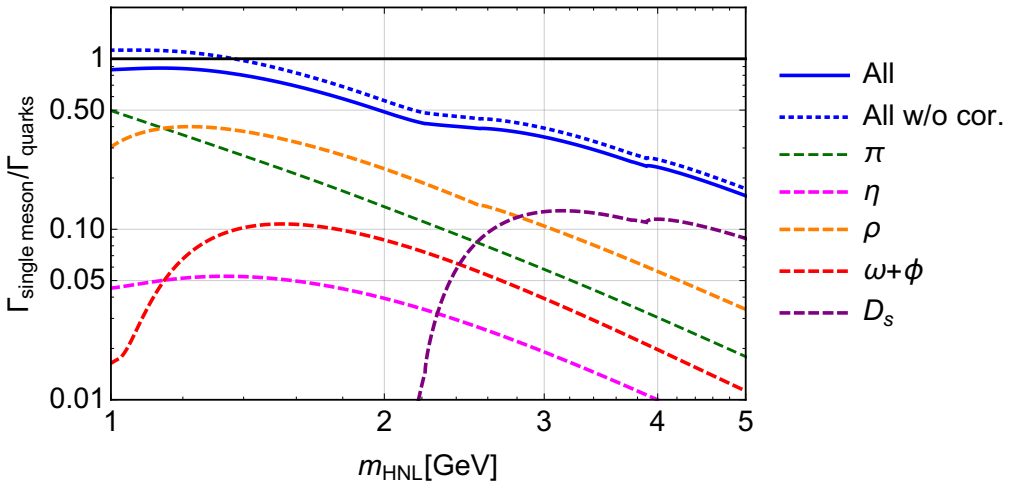

Figure 16. HNL decay widths into all relevant single meson channels, divided by the total decay width into quarks with QCD corrections, estimated as in (3.11) (all dashed lines). The blue solid line is the sum of the all mesons divided by decay width into quarks with QCD corrections, blue dotted line is the same but without QCD corrections.

3-body decays
$N \to \ell_\alpha^- \pi^+ \pi^0$
$N \to \nu_\alpha \pi^+ \pi^-$
$N \to \nu_\alpha \pi^0 \pi^0$
$N \to \ell_\alpha^- K^+ \bar{K}^0$
$N \to \nu_\alpha K^+ K^-$
$N \to \nu_\alpha K^0 \bar{K}^0$
$N \to \ell_\alpha^- K^+ \pi^0$
$N \to \ell_\alpha^- K^0 \pi^+$

4-body decays
$N \to \nu_\alpha (3\pi)^0$
$N \to \ell_\alpha^- (3\pi)^+$
$N \to \nu_\alpha (2\pi K)^0$
$N \to \ell_\alpha^- (2\pi K)^+$
$N \to \nu_\alpha (2K\pi)^0$
$N \to \ell_\alpha^- (2K\pi)^+$
$N \to \ell_\alpha^- (3K)^+$
$N \to \nu_\alpha (3K)^0$

Branching ratios $\tau^- \to \nu_\tau + X^-$	[%]
$\tau \to \nu_\tau + \pi^-$	10.8
$\tau \to \nu_\tau + \pi^- \pi^0$	25.5
$\tau \to \nu_\tau + \pi^0 \pi^- \pi^0$	9.2
$\tau \to \nu_\tau + \pi^- \pi^+ \pi^-$	9.0
$\tau \to \nu_\tau + \pi^- \pi^+ \pi^- \pi^0$	4.64
$\tau \to \nu_\tau + \pi^- \pi^0 \pi^0 \pi^0$	1.04
$\tau \to \nu_\tau + 5\pi$	$\mathcal{O}(1)$
$\tau \to \nu_\tau + K^-$ or $K^- \pi^0$	$\mathcal{O}(1)$
$\tau \to \nu_\tau + K^- K^0$	$\mathcal{O}(0.1)$
$\tau \to \nu_\tau + K^- K^0 \pi^0$	$\mathcal{O}(0.1)$

Table 4. Possible multi-meson decay channels of HNLs with $M_N > 2m_\pi$ threshold. Right panel shows branching ratios of hadronic decays of τ-lepton and demonstrates relative importance different hadronic 2, 3, 4 and 5 body channels.

give us information about decay through charged current of the HNL of the same mass as τ-lepton. The main difference between HNL and τ-lepton comes from the possibility of the HNL decay through the neutral current, which we discuss below.

As one observes, the main hadronic channels of the τ are n-pions channels. Decay channel into 2 pions is the most probable, but there is a large contribution from the 3 pions channels and still appreciable contribution from the 4 pions ones. For bigger masses the contribution from the channels with higher multiplicity become more important as figure 16 demonstrates.

The decay into kaons is suppressed for the τ-lepton. For some channels like $\tau \to \nu_\tau K$ or $\tau \to \nu_\tau K\pi$ this suppression comes from the Cabibbo angle between s and u quarks.

JHEP11(2018)032

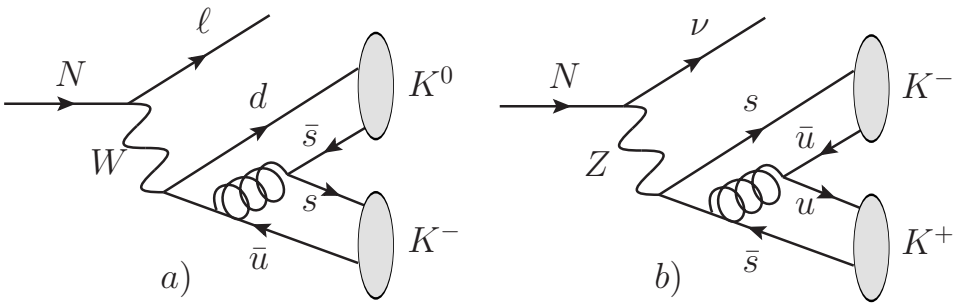

Figure 17. HNL decays into 2 kaons through charged a) and neutral b) currents.

The same argument holds for HNL decays into lepton and D meson, but not in D_s. The decays like $\tau \to \nu_\tau K^- K^0$ are not suppressed by CKM matrix and still are small. We think that this is because for such decays the probability of the QCD string fragmentation into strange quarks is much smaller than into u and d quarks for the given τ-lepton mass (see diagram a) in figure 17). At higher masses the probability of such fragmentation should be higher, but still too small to take it into account. On the other hand, the HNL decay into two kaons can give a noticeable contribution, because of existence of the neutral current decay (see diagram b) in figure 17), for which the previous arguments do not apply.

4 Summary

In this paper we revise the phenomenology of the heavy neutral leptons, including both their production and decays. We concentrated on the HNL masses up to $\mathcal{O}(10)$ GeV.

The mechanisms of the HNL production are secondary decays of the hadrons produced in the initial collision (section 2.1), production in proton-nucleon collision (section 2.3) and coherent scattering of the proton off nuclei (section 2.4). Of these mechanisms the production from the lightest flavored mesons dominate at all masses of interest. Production from baryons is not efficient at any HNL mass (see discussion in section 2.1.6). The main production channels above the kaon threshold are production from D mesons for $M_N \lesssim 2$ GeV and production from the beauty mesons for $M_N \lesssim m_\Upsilon$. For leptonic decays and two body semileptonic decays, the calculations are performed in appendix A. Our results agree with [51], for the case of the pseudoscalar and vector mesons we present the simplified version of the final formulas. We additionally analyzed the HNL production in B meson decays including multimeson final states, that were not previously discussed. We estimate that contribution of the multimeson final state give not more than 20% of production from B mesons (section 2.1.4).

The HNL are unstable and decay into light SM particles which can be detected. The HNL decay channels with branching ratio above 1% in the region $M_N < 5$ GeV are summarized in the table 5. For each channel we present the mass at which it opens, mass range where it is relevant and maximal branching ratio. The total decay width and the lifetime are summarized in figure 18.

JHEP11(2018)032

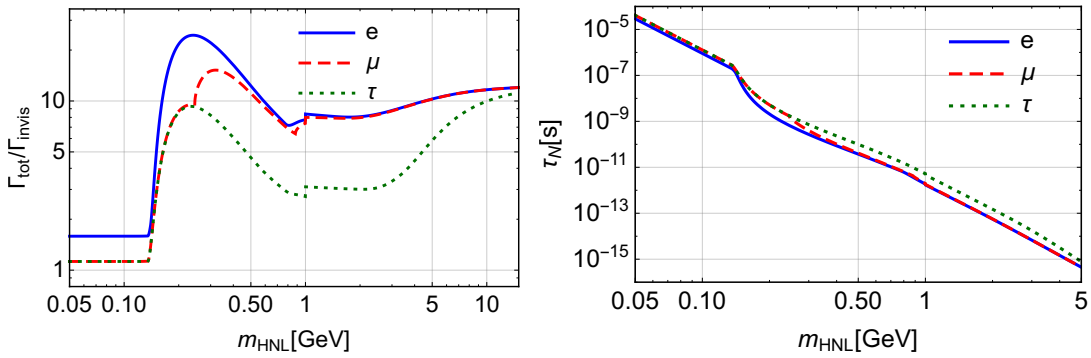

Figure 18. HNL decay width divided by the total decay width into active neutrinos eq. (3.5) (left panel) and lifetime (right panel) as a function of HNL mass. Results are given for the pure e, μ and τ mixings, $U_\alpha = 1$.

All HNL decay channels can be divided into purely leptonic and semileptonic (hadronic) ones. The decay widths into leptons are given by (3.1), (3.4), (3.5) and are in full agreement with the literature [51, 53].

For HNL masses above m_π semileptonic decay channels quickly start to dominate, the hardonic branching ratio reaches $\sim 70\%$ at $M_N \gtrsim 1\,\text{GeV}$. Single-meson final states (including decay into on-shell ρ mesons) saturate hadronic decay width till about 1.5 GeV (figure 16). In the HNL mass region $2-5\,\text{GeV}$ from 50% to 80% of the semileptonic decay width is saturated by multimeson states. For completeness we summarize all relevant hadronic form factors in appendices.

Our final results are directly suitable for sensitivity studies of particle physics experiments (ranging from proton beam-dump to the LHC) aiming at searches for heavy neutral leptons.

Acknowledgments

For this project K.B., A.B. and O.R. have received funding from the European Research Council (ERC) under the European Union's Horizon 2020 research and innovation programme (GA 694896) and from the Netherlands Science Foundation (NWO/OCW).

A HNL production from hadrons

The calculation of weak decays, involving hadrons is summarized in [83]. In the absence of QED and QCD corrections the effective weak interaction Lagrangian at low energies can be written as

$$\mathcal{L}_{\text{weak}} = \mathcal{L}_{\text{cc}} + \mathcal{L}_{\text{nc}} \tag{A.1}$$

where the *charged current* terms have the form

$$\mathcal{L}_{\text{cc}} = \frac{G_F}{\sqrt{2}} \left| \sum_{U,D} V_{UD} J^{\mu,+}_{UD} + \sum_{\ell} J^{\mu,+}_{\ell} \right|^2 , \tag{A.2}$$

JHEP11(2018)032

Channel	Opens at [MeV]	Relevant from [MeV]	Relevant to [MeV]	Max BR [%]	Reference in text
$N \to \nu_\alpha \nu_\beta \bar{\nu}_\beta$	$\sum m_\nu \approx 0$	$\sum m_\nu \approx 0$	—	100	(3.5)
$N \to \nu_\alpha e^+ e^-$	1.02	1.29	—	21.8	(3.4)
$N \to \nu_\alpha \pi^0$	135	136	3630	57.3	(3.7)
$N \to e^- \pi^+$	140	141	3000	33.5	(3.6)
$N \to \mu^- \pi^+$	245	246	3000	19.7	(3.6)
$N \to e^- \nu_\mu \mu^+$	106	315	—	5.15	(3.1)
$N \to \mu^- \nu_e e^+$	106	315	—	5.15	(3.1)
$N \to \nu_\alpha \mu^+ \mu^-$	211	441	—	4.21	(3.4)
$N \to \nu_\alpha \eta$	548	641	2330	3.50	(3.7)
$N \to e^- \pi^+ \pi^0$	275	666	4550	10.4	(B.42)
$N \to \nu_\alpha \pi^+ \pi^-$	279	750	3300	4.81	(B.43)
$N \to \mu^- \pi^+ \pi^0$	380	885	4600	10.2	(B.42)
$N \to \nu_\alpha \omega$	783	997	1730	1.40	(3.9)
$N \to \nu_\alpha (3\pi)^0$	$\gtrsim 405$	$\gtrsim 1000$	?	?	No
$N \to e^- (3\pi)^+$	$\gtrsim 410$	$\gtrsim 1000$	?	?	No
$N \to \nu_\alpha \eta'$	958	1290	2400	1.86	(3.7)
$N \to \nu_\alpha \phi$	1019	1100	4270	5.90	(3.9)
$N \to \mu^- (3\pi)^+$	$\gtrsim 515$	$\gtrsim 1100$	?	?	No
$N \to \nu_\alpha K^+ K^-$	987	$\gtrsim 1100$	?	?	No
$N \to \nu_\alpha (4\pi)^0$	$\gtrsim 540$	$\gtrsim 1200$	?	?	No
$N \to e^- (4\pi)^+$	$\gtrsim 545$	$\gtrsim 1200$	?	?	No
$N \to \mu^- (4\pi)^+$	$\gtrsim 649$	$\gtrsim 1300$	?	?	No
$N \to \nu_\alpha (5\pi)^0$	$\gtrsim 675$	$\gtrsim m_\tau \approx 1780$	?	?	No
$N \to e^- (5\pi)^+$	$\gtrsim 680$	$\gtrsim m_\tau \approx 1780$	?	?	No
$N \to \mu^- (5\pi)^+$	$\gtrsim 785$	$\gtrsim m_\tau \approx 1780$	?	?	No
$N \to e^- D_s^{*+}$	2110	2350	—	3.05	(3.8)
$N \to \mu^- D_s^{*+}$	2220	2370	—	3.03	(3.8)
$N \to e^- D_s^+$	1970	2660	4180	1.23	(3.6)
$N \to \mu^- D_s^+$	2070	2680	4170	1.22	(3.6)
$N \to \nu_\alpha \eta_c$	2980	3940	—	1.26	(3.7)
$N \to \tau^- \nu_e e^+$	1780	3980	—	1.52	(3.1)
$N \to e^- \nu_\tau \tau^+$	1780	3980	—	1.52	(3.1)
$N \to \tau^- \nu_\mu \mu^+$	1880	4000	—	1.51	(3.1)
$N \to \mu^- \nu_\tau \tau^+$	1880	4000	—	1.51	(3.1)

Table 5. Relevant HNL decay channels. Only channels with the branching ratio above 1% covering the HNL mass range up to 5 GeV are shown. The numbers are provided for $|U_e| = |U_\mu| = |U_\tau|$. For neutral current channels (with ν_a in the final state) the sum over neutrino flavors is taken, otherwise the lepton flavor is shown explicitly. *Columns*: (1) the HNL decay channel. Notation $(n\pi)^a$ means a system of n pions with the total charge a. (2) The HNL mass at which the channel opens; (3) The HNL mass starting from which the channel becomes relevant. For multimeson final states we provide our "best-guess estimates"; (4) HNL mass above which the channel contributes less than 1%; "—" means that the channel is still relevant at $M_N = 5$ GeV, "?" means that we could not estimate the relevance of the channel; (5) The maximal branching ratio of the channel for $M_N < 5$ GeV; (6) Reference to the formula for the decay width of the channel, if present in the text.

JHEP11(2018)032

where

$$J^{\mu,+}_{UD} = \bar{D}\gamma^{\mu}(1-\gamma^5)U, \tag{A.3}$$
$$J^{\mu,+}_{\ell} = \bar{\ell}\gamma^{\mu}(1-\gamma^5)\nu_{\ell}, \tag{A.4}$$

and V_{UD} is the CKM element which corresponds to quark flavour transition in hadronic current. For *neutral current* the interaction has the same form

$$\mathcal{L}_{\rm nc} = \frac{G_F}{\sqrt{2}}\left(\sum_f J^{\mu,0}_f\right)^2, \tag{A.5}$$

where summation goes over all fermions,

$$J^{\mu,0}_f = \bar{f}\gamma^{\mu}(v_f - a_f \qquad \gamma^5)f, \tag{A.6}$$
$$v_f = I_{3f} - 2Q_f \sin^2\theta_W, \qquad a_f = I_{3f} \tag{A.7}$$

and I_{3f} is the fermion isospin projection and Q_f is its electric charge ($Q_e = -1$). In the following sections we describe different processes with HNL and hadrons.

A.1 Leptonic decay of a pseudoscalar meson

Consider a decay of pseudoscalar meson h into charged lepton ℓ and HNL:

$$h \to \ell + N, \tag{A.8}$$

see left diagram in figure 2. The corresponding matrix element is given by

$$\mathcal{M} = \frac{G_F}{\sqrt{2}} V_{UD} \langle 0| J^{\mu}_{UD} |h\rangle \langle \ell, N| J_{\ell,\mu} |0\rangle, \tag{A.9}$$

where the corresponding quark contents of meson h is $|h\rangle = \left|\bar{U}D\right\rangle$. In order to fix the notations we remind that the charged meson coupling constant, f_h, for a pseudoscalar meson constructed from up (U) and down (D) type quarks is defined as

$$\langle 0| J^{\mu}_{UD} |h\rangle = \langle 0| \bar{U}\gamma^{\mu}\gamma_5 D |h\rangle \equiv i f_h p^{\mu} \tag{A.10}$$

where p_μ is 4-momentum of the pseudo-scalar meson h. The numerical values of the decay constants for different mesons are summarized in table 8.

After standard calculation one finds the decay width of this reaction

$$\Gamma(h \to \ell_\alpha N) = \frac{G_F^2 f_h^2 m_h^3}{8\pi} |V_{UD}|^2 |U_\alpha|^2 \left[y_N^2 + y_\ell^2 - \left(y_N^2 - y_\ell^2\right)^2\right] \sqrt{\lambda(1, y_N^2, y_\ell^2)}, \tag{A.11}$$

where $y_\ell = m_\ell/m_h$, $y_N = M_N/m_h$ and λ is given by (2.10).

JHEP11(2018)032

A.2 Semileptonic decay of a pseudoscalar meson

The process with pseudoscalar or vector meson $h'_{P/V}$ in the final state

$$h \to h'_{P/V} + \ell + N, \tag{A.12}$$

is mediated by the current that has $V-A$ form (see right diagram in figure 2). Properties of the hadronic matrix element $\left\langle h'_{P/V} \middle| J^{\mu}_{\text{hadron}} \middle| h \right\rangle$ depend on the type of final meson h' [84]. In the case of pseudoscalar meson only vector part of the current plays role:

$$\begin{aligned}\left\langle h'_P(p') \right| V_\mu \left| h(p) \right\rangle &= f_+(q^2)(p+p')_\mu + f_-(q^2)q_\mu \\ &= f_+(q^2)\left(p_\mu + p'_\mu - \frac{m_h^2 - m_{h'}^2}{q^2} q_\mu\right) + f_0(q^2)\frac{m_h^2 - m_{h'}^2}{q^2} q_\mu \end{aligned} \tag{A.13}$$

where $q_\mu = (p-p')_\mu$ is a transferred momentum and

$$f_0(q^2) \equiv f_+(q^2) + \frac{q^2}{m_h^2 - m_{h'}^2} f_-(q^2). \tag{A.14}$$

For the case of a vector meson h'_V in the final state both vector and axial part of the current contribute. The standard parametrization with form factors is

$$\left\langle h'_V(\epsilon, p'_\nu) \right| V^\mu \left| h(p_\nu) \right\rangle = ig(q^2)\varepsilon^{\mu\nu\sigma\rho}\epsilon^*_\nu (p+p')_\sigma (p-p')_\rho, \tag{A.15}$$

$$\left\langle h'_V(\epsilon, p'_\nu) \right| A_\mu \left| h(p_\nu) \right\rangle = f(q^2)\epsilon^*_\mu + a_+(q^2)(\epsilon^* \cdot p)(p+p')_\mu + a_-(q^2)(\epsilon^* \cdot p)(p-p')_\mu, \tag{A.16}$$

where ϵ_μ is a polarization vector of the vector meson h'_V.

Using matrix elements (A.13)–(A.16) it is straightforward to calculate decay widths of the reactions. In the case of pseudoscalar meson h'_P we follow ref. [55] and decompose full decay width into 4 parts,

$$\Gamma(h \to h'_P \ell_\alpha N) = \frac{G_F^2 m_h^5}{64\pi^3} C_K^2 |V_{UD}|^2 |U_\alpha|^2 \left(I_{P,1} + I_{P,2} + I_{P,3} + I_{P,4}\right), \tag{A.17}$$

where $I_{P,1}, I_{P,2}$ depend on $|f_+(q^2)|^2$, $I_{P,3}$ on $|f_0(q^2)|^2$ and $I_{P,4}$ on $\mathrm{Re}\left(f_0(q^2) f_+^*(q^2)\right)$. It turns out that $I_{P,4} = 0$, the explicit expressions for others are

$$I_{P,1} = \int_{(y_\ell + y_N)^2}^{(1-y_{h'})^2} \frac{d\xi}{3\xi^3} |f_+(q^2)|^2 \Lambda^3(\xi), \tag{A.18}$$

$$I_{P,2} = \int_{(y_\ell + y_N)^2}^{(1-y_{h'})^2} \frac{d\xi}{2\xi^3} |f_+(q^2)|^2 \Lambda(\xi) G_-(\xi) \lambda(1, y_{h'}^2, \xi), \tag{A.19}$$

$$I_{P,3} = \int_{(y_\ell + y_N)^2}^{(1-y_{h'})^2} \frac{d\xi}{2\xi^3} |f_0(q^2)|^2 \Lambda(\xi) G_-(\xi) (1 - y_{h'}^2)^2, \tag{A.20}$$

where

$$\Lambda(\xi) = \lambda^{1/2}(1, y_{h'}^2, \xi) \lambda^{1/2}(\xi, y_N^2, y_\ell^2), \tag{A.21}$$

$$G_-(\xi) = \xi\left(y_N^2 + y_\ell^2\right) - \left(y_N^2 - y_\ell^2\right)^2, \tag{A.22}$$

JHEP11(2018)032

$y_i = \frac{m_i}{m_h}$, $\xi = \frac{q^2}{m_h^2}$ and function $\lambda(a,b,c)$ is given by (2.10). C_K is a Clebsh-Gordan coefficient, see for example [85, (14)] and [86, (2.1)], $C_K = 1/\sqrt{2}$ for decays into π^0 and $C_K = 1$ for all other cases.

For the decay into vector meson the expression is more bulky,

$$\Gamma(h \to h'_V \ell_\alpha N) = \frac{G_F^2 m_h^7}{64\pi^3 m_{h'}^2} C_K^2 |V_{UD}|^2 |U_\alpha|^2 \Big(I_{V,g^2} + I_{V,f^2} + I_{V,a_+^2} + I_{V,a_-^2} + I_{V,gf} + I_{V,ga_+} + I_{V,ga_-} + I_{V,fa_+} + I_{V,fa_-} + I_{V,a_+a_-} \Big), \tag{A.23}$$

where $I_{V,FG}$ are parts of the decay width that depend on the FG form factors combination[9] and C_K is a Clebsh-Gordan coefficient, $C_K = 1/\sqrt{2}$ for decays into ρ^0 and $C_K = 1$ for all other cases in this paper. It turns out that $I_{V,gf} = I_{V,ga_+} = I_{V,ga_-} = 0$, the other terms are given by

$$I_{V,g^2} = \frac{m_h^2 y_{h'}^2}{3} \int_{(y_\ell + y_N)^2}^{(1-y_{h'})^2} \frac{d\xi}{\xi^2} g^2(q^2) \Lambda(\xi) F(\xi) \left(2\xi^2 - G_+(\xi)\right), \tag{A.24}$$

$$I_{V,f^2} = \frac{1}{24 m_h^2} \int_{(y_\ell + y_N)^2}^{(1-y_{h'})^2} \frac{d\xi}{\xi^3} f^2(q^2) \Lambda(\xi) \times \left(3F(\xi) \left[\xi^2 - \left(y_\ell^2 - y_N^2\right)^2 \right] - \Lambda^2(\xi) + 12 y_{h'}^2 \xi \left[2\xi^2 - G_+(\xi)\right] \right), \tag{A.25}$$

$$I_{V,a_+^2} = \frac{m_h^2}{24} \int_{(y_\ell + y_N)^2}^{(1-y_{h'})^2} \frac{d\xi}{\xi^3} a_+^2(q^2) \Lambda(\xi) F(\xi) \left(F(\xi) \left[2\xi^2 - G_+(\xi)\right] + 3 G_-(\xi) \left[1 - y_{h'}^2\right]^2 \right), \tag{A.26}$$

$$I_{V,a_-^2} = \frac{m_h^2}{8} \int_{(y_\ell + y_N)^2}^{(1-y_{h'})^2} \frac{d\xi}{\xi} a_-^2(q^2) \Lambda(\xi) F(\xi) G_-(\xi), \tag{A.27}$$

$$I_{V,fa_+} = \frac{1}{12} \int_{(y_\ell + y_N)^2}^{(1-y_{h'})^2} \frac{d\xi}{\xi^3} f(q^2) a_+(q^2) \Lambda(\xi) \times \left(3\xi F(\xi) G_-(\xi) + \left(1 - \xi - y_{h'}^2\right) \left[3F(\xi) \left(\xi^2 - \left(y_l^2 - y_N^2\right)^2 \right) - \Lambda^2(\xi) \right] \right), \tag{A.28}$$

$$I_{V,fa_-} = \frac{1}{4} \int_{(y_\ell + y_N)^2}^{(1-y_{h'})^2} \frac{d\xi}{\xi^2} f(q^2) a_-(q^2) \Lambda(\xi) F(\xi) G_-(\xi), \tag{A.29}$$

$$I_{V,a_+a_-} = \frac{m_h^2}{4} \int_{(y_\ell + y_N)^2}^{(1-y_{h'})^2} \frac{d\xi}{\xi^2} a_+(q^2) a_-(q^2) \Lambda(\xi) F(\xi) G_-(\xi) \left(1 - y_{h'}^2\right), \tag{A.30}$$

where the notation is the same as in eqs. (A.18)–(A.20) and

$$F(\xi) = (1-\xi)^2 - 2y_{h'}^2(1+\xi) + y_{h'}^4, \tag{A.31}$$

$$G_+(\xi) = \xi \left(y_N^2 + y_\ell^2\right) + \left(y_N^2 - y_\ell^2\right)^2. \tag{A.32}$$

[9] In this computation we take all form factors as real-valued functions.

JHEP11(2018)032

B HNL decays into hadronic states

B.1 Connection between matrix elements of the unflavoured mesons

B.1.1 G-symmetry

An important symmetry of the low-energy theory of strong interactions is the so-called *G-symmetry* which is a combination of the charge conjugation $\hat{C}$ and rotation of 180° around the y axis in the isotopic space $\hat{R}_y$.[10] The operation of charge conjugation acts on bilinear combinations of fermions f_1, f_2 as follows:

$$\hat{C}\bar{f}_1 f_2 = \bar{f}_2 f_1, \tag{B.1}$$
$$\hat{C}\bar{f}_1\gamma_5 f_2 = \bar{f}_2\gamma_5 f_1, \tag{B.2}$$
$$\hat{C}\bar{f}_1\gamma_\mu f_2 = -\bar{f}_2\gamma_\mu f_1, \tag{B.3}$$
$$\hat{C}\bar{f}_1\gamma_\mu\gamma_5 f_2 = \bar{f}_2\gamma_\mu\gamma_5 f_1. \tag{B.4}$$

$\hat{R}_y$ acts on the isospin doublet as

$$\hat{R}_y \begin{pmatrix} u \\ d \end{pmatrix} = \begin{pmatrix} d \\ -u \end{pmatrix}. \tag{B.5}$$

Acting on pion states, that are pseudoscalar isovectors, one gets

$$\hat{G}\left|\pi^+\right\rangle = \hat{R}_y\hat{C}\left|\bar{d}\gamma_5 u\right\rangle = \hat{R}_y\left|\bar{u}\gamma_5 d\right\rangle = -\left|\bar{d}\gamma_5 u\right\rangle = -\left|\pi^+\right\rangle, \tag{B.6}$$
$$\begin{aligned}\hat{G}\left|\pi^0\right\rangle &= \hat{R}_y\hat{C}\frac{1}{\sqrt{2}}\left|\bar{u}\gamma_5 u - \bar{d}\gamma_5 d\right\rangle = \hat{R}_y\frac{1}{\sqrt{2}}\left|\bar{u}\gamma_5 u - \bar{d}\gamma_5 d\right\rangle \\ &= -\frac{1}{\sqrt{2}}\left|\bar{u}\gamma_5 u - \bar{d}\gamma_5 d\right\rangle = -\left|\pi^0\right\rangle,\end{aligned} \tag{B.7}$$

so any pion is an odd state under G-symmetry. As a consequence, for the system of n pions

$$\hat{G}\left|n\pi\right\rangle = (-1)^n\left|n\pi\right\rangle. \tag{B.8}$$

For ρ mesons, which are vector isovectors, G-parity is positive,

$$\hat{G}\left|\rho^+\right\rangle = \hat{R}_y\hat{C}\left|\bar{d}\gamma_\mu u\right\rangle = -\hat{R}_y\left|\bar{u}\gamma_\mu d\right\rangle = \left|\bar{d}\gamma_\mu u\right\rangle = \left|\rho^+\right\rangle, \tag{B.9}$$
$$\begin{aligned}\hat{G}\left|\rho^0\right\rangle &= \hat{R}_y\hat{C}\frac{1}{\sqrt{2}}\left|\bar{u}\gamma_\mu u - \bar{d}\gamma_\mu d\right\rangle = -\hat{R}_y\frac{1}{\sqrt{2}}\left|\bar{u}\gamma_\mu u - \bar{d}\gamma_\mu d\right\rangle \\ &= \frac{1}{\sqrt{2}}\left|\bar{u}\gamma_\mu u - \bar{d}\gamma_\mu d\right\rangle = \left|\rho^0\right\rangle,\end{aligned} \tag{B.10}$$

while for a_1 mesons, which are pseudovector isovectors, G-parity is negative,

$$\hat{G}\left|a_1^+\right\rangle = \hat{R}_y\hat{C}\left|\bar{d}\gamma_\mu\gamma_5 u\right\rangle = \hat{R}_y\left|\bar{u}\gamma_\mu\gamma_5 d\right\rangle = -\left|\bar{d}\gamma_\mu\gamma_5 u\right\rangle = -\left|a_1^+\right\rangle, \tag{B.11}$$
$$\begin{aligned}\hat{G}\left|a_1^0\right\rangle &= \hat{R}_y\hat{C}\frac{1}{\sqrt{2}}\left|\bar{u}\gamma_\mu\gamma_5 u - \bar{d}\gamma_\mu\gamma_5 d\right\rangle = \hat{R}_y\frac{1}{\sqrt{2}}\left|\bar{u}\gamma_\mu\gamma_5 u - \bar{d}\gamma_\mu\gamma_5 d\right\rangle \\ &= -\frac{1}{\sqrt{2}}\left|\bar{u}\gamma_\mu\gamma_5 u - \bar{d}\gamma_\mu\gamma_5 d\right\rangle = -\left|a_1^0\right\rangle,\end{aligned} \tag{B.12}$$

[10] The latter corresponds to the interchange of u and d quarks with an additional phase, see eq. (B.5) below.

JHEP11(2018)032

Current	$j_\mu^{V,s}$	$j_\mu^{V,+/0/-}$	$j_\mu^{A,s}$	$j_\mu^{A,+/0/-}$
G-parity	$-$	$+$	$+$	$-$

Table 6. Properties of axial and vector currents under G-symmetry.

B.1.2 Classification of currents

Unflavoured quarks system interacts with electromagnetic field, W- and Z-bosons through currents

$$J_\mu^{\rm EM} = \frac{2}{3}\bar{u}\gamma_\mu u - \frac{1}{3}\bar{d}\gamma_\mu d, \tag{B.13}$$

$$J_\mu^{W} = \bar{u}\gamma_\mu(1-\gamma_5)d, \tag{B.14}$$

$$J_\mu^{Z} = \bar{u}\gamma_\mu(v_u - a_u\gamma_5)u + \bar{d}\gamma_\mu(v_d - a_d\gamma_5)d, \tag{B.15}$$

where

$$v_u = \frac{1}{2} - \frac{4}{3}\sin^2\theta_W, \qquad a_u = \frac{1}{2}, \tag{B.16}$$

$$v_d = -\frac{1}{2} + \frac{2}{3}\sin^2\theta_W, \qquad a_d = -\frac{1}{2}. \tag{B.17}$$

To divide currents (B.13)–(B.15) into G-odd and G-even parts let us introduce isoscalar and isovector vector currents

$$j_\mu^{V,s} = \frac{1}{\sqrt{2}}(\bar{u}\gamma_\mu u + \bar{d}\gamma_\mu d), \tag{B.18}$$

$$j_\mu^{V,0} = \frac{1}{\sqrt{2}}(\bar{u}\gamma_\mu u - \bar{d}\gamma_\mu d), \tag{B.19}$$

$$j_\mu^{V,+} = \bar{d}\gamma_\mu u\,, \qquad j_\mu^{V,-} = \bar{u}\gamma_\mu d\,, \tag{B.20}$$

and isoscalar and isovector axial currents

$$j_\mu^{A,s} = \frac{1}{\sqrt{2}}(\bar{u}\gamma_\mu\gamma_5 u + \bar{d}\gamma_\mu\gamma_5 d), \tag{B.21}$$

$$j_\mu^{A,0} = \frac{1}{\sqrt{2}}(\bar{u}\gamma_\mu\gamma_5 u - \bar{d}\gamma_\mu\gamma_5 d), \tag{B.22}$$

$$j_\mu^{A,+} = \bar{d}\gamma_\mu\gamma_5 u\,, \qquad j_\mu^{A,-} = \bar{u}\gamma_\mu\gamma_5 d\,. \tag{B.23}$$

Currents (B.18)–(B.23) have certain G-parity presented in table 6. Using these currents one can rewrite physical currents as

$$J_\mu^{\rm EM} = \frac{1}{\sqrt{2}}j_\mu^{V,0} + \frac{1}{3\sqrt{2}}j_\mu^{V,s}, \tag{B.24}$$

$$J_\mu^{W} = j_\mu^{V,-} - j_\mu^{A,-}, \tag{B.25}$$

$$J_\mu^{Z} = \frac{1-2\sin^2\theta_W}{\sqrt{2}}j_\mu^{V,0} - \frac{\sqrt{2}\sin^2\theta_W}{3}j_\mu^{V,s} - \frac{1}{\sqrt{2}}j_\mu^{A,0}. \tag{B.26}$$

JHEP11(2018)032

B.1.3 Connection between matrix elements

G-even part of currents (B.24)–(B.26) belongs to one isovector family, therefore there is an approximate connection between matrix elements for the system of even number of pions or ρ-meson,

$$\langle 0|\, J_\mu^{\rm EM}\, |2n\pi/\rho\rangle \approx \frac{1}{\sqrt{2}} \langle 0|\, J_\mu^{W}\, |2n\pi/\rho\rangle \approx \frac{1}{1-2\sin^2\theta_W} \langle 0|\, J_\mu^{Z}\, |2n\pi/\rho\rangle\,. \tag{B.27}$$

The special case to mention here is $\left|2\pi^0\right\rangle$ state. In $V\pi^0\pi^0$ vertex, where $V=\gamma/Z$, system of 2 pions should have total angular momentum $J=1$. Pions are spinless particles, so their coordinate wavefuction has negative parity, which is forbidden by the Bose-Einstein statistics. Therefore

$$\langle 0|\, J_\mu^{\rm EM}\, \left|2\pi^0\right\rangle = \langle 0|\, J_\mu^{Z}\, \left|2\pi^0\right\rangle = 0. \tag{B.28}$$

This result is equivalent to the prohibition of the $\rho^0 \to 2\pi^0$ decay.

G-odd parts of the currents (B.24)–(B.26), see table 6, belong to one isoscalar and one isovector families, so there is only one relation between matrix elements for the system of odd number of pions or for a_1-mesons,

$$\frac{1}{\sqrt{2}} \langle 0|\, J_\mu^{W}\, |(2n+1)\pi/a_1\rangle \approx \langle 0|\, J_\mu^{Z}\, |(2n+1)\pi/a_1\rangle + 2\sin^2\theta_W \langle 0|\, J_\mu^{\rm EM}\, |(2n+1)\pi/a_1\rangle\,. \tag{B.29}$$

The last formula can be simplified in the case of the one-pion or a_1 state. The direct interaction between photon and π^0 is forbidden because of the C symmetry, while photon-to-a_1 interaction violates both P and C symmetry. Therefore, the matrix element $\langle 0|\, J_\mu^{\rm EM}\, |\pi/a_1\rangle = 0$ and

$$\frac{1}{\sqrt{2}} \langle 0|\, J_\mu^{W}\, |\pi/a_1\rangle \approx \langle 0|\, J_\mu^{Z}\, |\pi/a_1\rangle\,. \tag{B.30}$$

All the approximate relations discussed above hold up to isospin violating terms of order $(m_{\pi^+} - m_{\pi^0})/m_\pi \sim 3.4\%$.

B.2 HNL decays to a meson and a lepton

There are 4 types of this decay: $N \to \ell_\alpha + h_{P/V}$ and $N \to \nu_\alpha + h_{P/V}$, where h_P and h_V are pseudoscalar and vector mesons respectively. Reaction $N \to \ell_\alpha + h_P$ is closely related to the process calculated in section A.1. It utilizes the same matrix element and differs only by kinematics. Using the same notation, the decay width is

$$\Gamma(N \to \ell_\alpha h_P) = \frac{G_F^2 f_h^2 M_N^3}{16\pi} |V_{UD}|^2 |U_\alpha|^2 \left[\left(1-x_\ell^2\right)^2 - x_h^2(1+x_\ell^2)\right] \sqrt{\lambda(1,x_h^2,x_\ell^2)}, \tag{B.31}$$

where $x_h = m_h/M_N$, $x_\ell = m_\ell/M_N$ and function λ is given by eq. (2.10).

In case of the neutral current-mediated decay $N \to \nu_\alpha + h_P$ the hadronic matrix element reads (see section C.1.1 for details)

$$\langle 0|\, J_\mu^{Z}\, \left|h_P^0\right\rangle \equiv -i\frac{f_h}{\sqrt{2}} p_\mu, \tag{B.32}$$

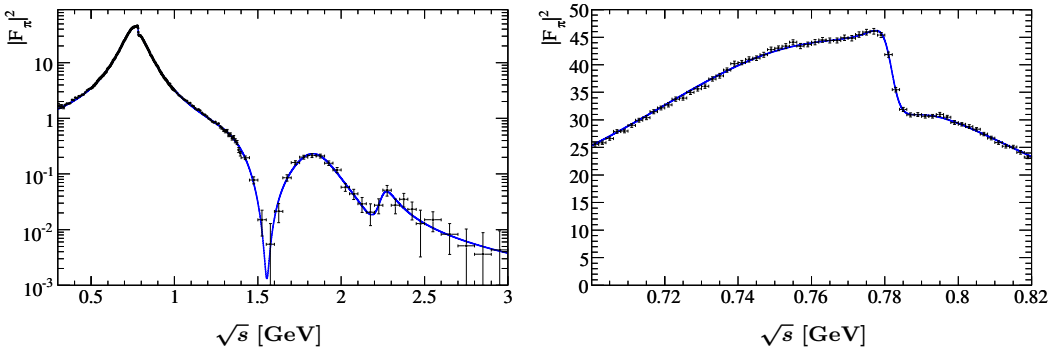

Figure 19. Pion form factor squared, $|F_\pi|^2$. *Left:* fit to the BaBaR data [87] using the vector-dominance model (blue line). *Right:* zoom to the energies around $\sqrt{s} \simeq m_\rho$.

where p_μ is the 4-momentum of the pseudo-scalar meson h, J^Z_μ current is given by eq. (B.15). The decay width is

$$\Gamma(N \to \nu_\alpha h_P) = \frac{G_F^2 f_h^2 M_N^3}{32\pi} |U_\alpha|^2 \left(1 - x_h^2\right)^2, \tag{B.33}$$

where $x_h = m_h/M_N$ and f_h are neutral meson decay constants presented in the right part of table 8.

Consider the process $N \to \ell_\alpha + h_V$. For the vector meson the hadronic matrix element of the charged current is defined as

$$\langle 0| J^\mu_{UD} |h_V\rangle \equiv i g_h \varepsilon^\mu(p), \tag{B.34}$$

where $\varepsilon^\mu(p)$ is polarization vector of the meson and g_h is the vector meson decay constant. The values of the g_h are given in table 9. Using previous notations, the decay width of this process is

$$\Gamma(N \to \ell^-_\alpha h^+_V) = \frac{G_F^2 g_h^2 |V_{UD}|^2 |U_\alpha|^2 M_N^3}{16\pi m_h^2} \left(\left(1 - x_\ell^2\right)^2 + x_h^2\left(1 + x_\ell^2\right) - 2x_h^4\right) \sqrt{\lambda(1, x_h^2, x_\ell^2)}. \tag{B.35}$$

Finally, to calculate HNL decay into neutral vector meson $N \to \nu_\alpha + h_V$ we define the hadronic matrix element as

$$\langle 0| J^Z_\mu \left|h^0_V\right\rangle \equiv i \frac{\kappa_h g_h}{\sqrt{2}} \varepsilon^\mu(p), \tag{B.36}$$

where g_h is the vector meson decay constant and κ_h is dimensionless correction factor, their values are given in table 9. For the decay width one obtains

$$\Gamma(N \to \nu_\alpha h_V) = \frac{G_F^2 \kappa_h^2 g_\rho^2 |U_\alpha|^2 M_N^3}{32\pi m_h^2} \left(1 + 2x_h^2\right)\left(1 - x_h^2\right)^2. \tag{B.37}$$

B.3 HNL decays to a lepton and two pions

For the case of 2 pions the matrix element of the axial current is equal to zero, so the general expression for matrix element is (cf. (A.13))

$$\left\langle \pi(p')\right| J_\mu \left|\pi(p)\right\rangle = f_+(q^2)(p + p')_\mu + f_-(q^2) q_\mu, \tag{B.38}$$

JHEP11(2018)032

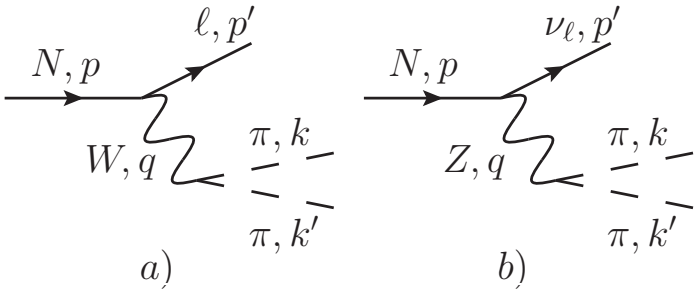

Figure 20. Diagram for the HNL decay into 2 pions.

where J_μ is one of the currents (B.13)–(B.15) and $q_\mu = (p - p')_\mu$. Because of isospin symmetry (B.27) the form factors are related as

$$f_\pm^{\rm EM} \approx \frac{1}{\sqrt{2}} f_\pm^W \approx \frac{1}{1 - 2\sin^2\theta_W} f_\pm^Z \tag{B.39}$$

Electromagnetic current conservation $q_\mu J^\mu = 0$ implies $f_-^{\rm EM}(q^2) = 0$. Therefore all the matrix elements could be expressed via only one form factor, called *pion electromagnetic form factor*,

$$\langle \pi(p') | J_\mu^{\rm EM} | \pi(p) \rangle = F_\pi(q^2)(p + p')_\mu. \tag{B.40}$$

Pion electromagnetic form factor is related to the cross section of reaction $e^+e^- \to 2\pi$ as

$$\sigma(e^+e^- \to 2\pi) = \frac{\pi\alpha_{\rm EM}^2}{3s}\beta_\pi^3(s)|F_\pi(s)|^2, \tag{B.41}$$

where $\beta_\pi(s) = \sqrt{1 - 4m_\pi^2/s}$, so it is well-measured experimentally. There are a lot of data on electromagnetic form factor [87–92], which agree with each other. Good description of the data is given by the vector-dominance model (VDM), see figure 19 [87] and appendix F for model description.

Using matrix elements described above it is easy to find the decay widths of $N \to \ell\pi^0\pi^+$ and $N \to \nu_\ell\pi^+\pi^-$ (see Feynman diagrams in figure 20),

$$\begin{aligned}\Gamma(N \to \ell_\alpha\pi^0\pi^+) = {} & \frac{G_F^2 M_N^3}{384\pi^3}|V_{ud}|^2|U_\alpha|^2 \int_{4m_\pi^2}^{(M_N - m_\ell)^2} \left((1 - x_\ell^2)^2 + \frac{q^2}{M_N^2}(1 + x_\ell^2) - 2\frac{q^4}{M_N^4}\right) \\ & \times \lambda^{1/2}\left(1, \frac{q^2}{M_N^2}, x_\ell^2\right)\beta_\pi^3(q^2)|F_\pi(q^2)|^2 dq^2, \end{aligned} \tag{B.42}$$

$$\begin{aligned}\Gamma(N \to \nu_\alpha\pi^+\pi^-) = {} & \frac{G_F^2 M_N^3}{768\pi^3}|U_\alpha|^2(1 - 2\sin^2\theta_W)^2 \\ & \times \int_{4m_\pi^2}^{M_N^2} \left(1 - \frac{q^2}{M_N^2}\right)^2 \left(1 + \frac{2q^2}{M_N^2}\right)\beta_\pi^3(q^2)|F_\pi(q^2)|^2 dq^2, \end{aligned} \tag{B.43}$$

where $x_\ell = \dfrac{m_\ell}{M_N}$ and the function λ is given by (2.10). The decay width $\Gamma(N \to \nu_\alpha\pi^0\pi^0) = 0$ because of eq. (B.28).

JHEP11(2018)032

V_{ud}	V_{us}	V_{ub}	V_{cd}	V_{cs}	V_{cb}
0.974	0.225	0.00409	0.220	0.995	0.0405

Table 7. CKM matrix elements [65] adopted in this work.

Using VDM model, formula (B.42) and lifetime of the τ-lepton we have calculated the branching ratio $\mathrm{BR}(\tau \to \nu_\tau \pi^- \pi^0) = 25.2\%$ which is close to the experimental value 25.5%.

The decay into 2 pions is significantly enhanced by the ρ-resonance. It turns out, that this is the dominant channel, see figure 15 with comparison of the decay width of HNL into 2 pions and into ρ-meson. Therefore, one can replace the decay into 2 pions with 2-body decay into ρ-meson.

C Phenomenological parameters

In this section we summarize parameters used in this work. Values of the CKM matrix elements are given in table 7.

C.1 Meson decay constants

The decay constants for charged pseudoscalar mesons are defined by eq. (A.10), Values of f_h (table 8) are measured experimentally and/or obtained by lattice calculations [93].

Meson decay constants for the mesons with the same-flavour quarks are defined by eq. (B.32). There is a discrepancy regarding their values in the literature, therefore we have computed them directly (see appendix C.1.1). The results of these computations are given in the right column of table 8. The meson decay constants for neutral mesons consisted of quarks of different flavors (such as K^0, D^0, B^0, B_s) are not needed in computing HNL production or decay, we do not provide them here.

For vector charged mesons the decay constants g_h are defined by eq. (B.34). In the literature they often appear as f_h, connected to our prescription by mass of the meson $g_h = f_h m_h$. Their values are presented in table 9. For vector neutral mesons the decay constants g_h and dimensionless factors κ_h are defined by eq. (B.36). Their values are presented in table 9 as well.

C.1.1 Decay constants of η and η' mesons

To describe HNL decays into η and η' mesons we need to know the corresponding neutral current decay constants, that we define as (B.32)

$$\langle 0 | J^Z_\mu | h^0_P \rangle \equiv -i \frac{f_h}{\sqrt{2}} p_\mu,$$

where where p_μ is the 4-momentum of the pseudo-scalar meson h, J^Z_μ current is given by eq. (B.15). The choice of the additional factor $(-1/\sqrt{2})$ is introduced in order to obtain $f_{\pi^0} = f_{\pi^\pm}$ and $f_{\pi^0} > 0$, see discussion below. Taking into account that for pseudoscalar

JHEP11(2018)032

f_{π^+}	130.2 MeV [93]
f_{K^+}	155.6 MeV [93]
f_{D^+}	212 MeV [93]
f_{D_s}	249 MeV [93]
f_{B^+}	187 MeV [93]
f_{B_c}	434 MeV [94]

f_{π^0}	130.2 MeV [(a)]
f_η	81.7 MeV [(b)]
$f_{\eta'}$	−94.7 MeV [(b)]
f_{η_c}	237 MeV [(c)]

[(a)]: it should be equal to f_{π^+}, according to eq. (B.30).
[(b)]: see discussion in section C.1.1.
[(c)]: see discussion in section C.1.2.

Table 8. Decay constants of pseudoscalar charged mesons (left table) and pseudoscalar neutral mesons (right table).

g_{ρ^+}	0.162 GeV^2 [95] [(a)]
$g_{D^{+*}}$	0.535 GeV^2 [96]
$g_{D_s^{+*}}$	0.650 GeV^2 [96]

h	g_h [GeV^2]	κ_h
ρ^0	0.162	$1-2\sin^2\theta_W$ [(b)]
ω	0.153 [53]	$\frac{4}{3}\sin^2\theta_W$
ϕ	0.234 [95]	$\frac{4}{3}\sin^2\theta_W - 1$
J/ψ	1.29 [97]	$1-\frac{8}{3}\sin^2\theta_W$

[(a)]: see discussion in the section C.1.3.
[(b)]: see eq. (B.27).

Table 9. Decay constants of vector charged mesons (left table) and vector neutral mesons (right table). Decay constants for $D^*_{(s)}$ mesons in [96] show large theoretical uncertainty, we quote only the average value here.

mesons only axial part of the current contributes to this matrix element we can write the matrix element as

$$\langle 0|\, J^Z_\mu \,|h^0_P\rangle = \langle 0|\, \bar{q}\gamma_\mu\gamma^5\lambda^Z q \,|h^0_P\rangle\,, \tag{C.1}$$

where

$$q = \begin{pmatrix} u \\ d \\ s \end{pmatrix}, \qquad \lambda^Z = \frac{1}{2}\begin{pmatrix} -1 & 0 & 0 \\ 0 & 1 & 0 \\ 0 & 0 & 1 \end{pmatrix}. \tag{C.2}$$

The relevant decay constants are f^0 and f^8, they come from the set of extracted from experiments decay constants defined as [98]

$$\langle 0|\, J^a_\mu \,|h\rangle = i f^a_h p_\mu, \tag{C.3}$$

where $J^a_\mu = \bar{q}\gamma_\mu\gamma^5\dfrac{\lambda^a}{\sqrt{2}}q$ with λ^a being the Gell-Mann matrices for $a = 1\ldots 8$ and

$$\lambda^0 = \sqrt{\frac{2}{3}}\begin{pmatrix} 1 & 0 & 0 \\ 0 & 1 & 0 \\ 0 & 0 & 1 \end{pmatrix} \tag{C.4}$$

The overall factor in λ^0 is chosen to obey normalization condition $\mathrm{Tr}(\lambda^a\lambda^b) = 2\delta^{ab}$.

JHEP11(2018)032

Within the chiral perturbation theory (χPT) (see [99] and references therein), the lightest mesons corresponds to pseudogoldstone bosons ϕ^a, that appear after the spontaneous breaking of $U_L(3) \times U_R(3)$ symmetry to group $U_V(3)$. States ϕ^a are orthogonal in the sense

$$\langle 0| J^a_\mu \left|\phi^b\right\rangle = i f^a_{\phi^b} p_\mu, \quad f^a_{\phi^b} = f^a_b \delta^{ab} \tag{C.5}$$

where and f^a_b are corresponding decay constants. Using

$$\lambda^3 = \begin{pmatrix} 1 & 0 & 0 \\ 0 & -1 & 0 \\ 0 & 0 & 0 \end{pmatrix}, \qquad \lambda^8 = \sqrt{\frac{1}{3}} \begin{pmatrix} 1 & 0 & 0 \\ 0 & 1 & 0 \\ 0 & 0 & -2 \end{pmatrix}, \tag{C.6}$$

we can rewrite the axial part of the weak neutral current (B.32) as a linear combination of the J^0_μ, J^3_μ and J^8_μ

$$\bar{q}\gamma_\mu\gamma^5\lambda^Z q = \frac{1}{\sqrt{2}} \left(\frac{J^0_\mu}{\sqrt{6}} - \frac{J^8_\mu}{\sqrt{3}} - J^3_\mu \right) \tag{C.7}$$

and f_h is given by

$$f_h = f^3_h + \frac{f^8_h}{\sqrt{3}} - \frac{f^0_h}{\sqrt{6}}. \tag{C.8}$$

For example, π^0 meson corresponds to ϕ^3 state in χPT, so $f^0_{\pi^0} = f^8_{\pi^0} = 0$ and eq. (C.8) gives $f_{\pi^0} = f^3_{\pi^0} = f_{\pi^+}$ because of isospin symmetry, in full agreement with eq. (B.30).

For η and η' application of eq. (C.8) is not so straightforward. These mesons are neutral unflavoured mesons with zero isospin and they can oscillate between each other. So η and η' do not coincide with any single ϕ^a state. Rather they are mixtures of ϕ^0 and ϕ^8 states. In real world isospin is not a conserved quantum number, so ϕ^3 state also should be taken into account, but its contribution is negligible [100], so we use $f^3_\eta = f^3_{\eta'} = 0$. Another complication is U(1) QCD anomaly for J^0_μ current that not only shifts masses of corresponding mesons but also contributes to f^0_h meson constant. To phenomenologically take into account the effect of anomaly it was proposed to use two mixing angles scheme [101],

$$\begin{pmatrix} f^8_\eta & f^0_\eta \\ f^8_{\eta'} & f^0_{\eta'} \end{pmatrix} = \begin{pmatrix} f_8 \cos\theta_8 & -f_0 \sin\theta_0 \\ f_8 \sin\theta_8 & f_0 \cos\theta_0 \end{pmatrix}. \tag{C.9}$$

Taking parameter values from the recent phenomenological analysis [98],

$$f_8 = 1.27(2) f_\pi, \quad f_0 = 1.14(5) f_\pi, \quad \theta_8 = -21.2(1.9)^\circ, \quad \theta_0 = -6.9(2.4)^\circ, \tag{C.10}$$

we find

$$f_\eta = 0.63(2) f_\pi \approx 81.7(3.1)\ \text{MeV}, \tag{C.11}$$

$$f_{\eta'} = -0.73(3) f_\pi \approx -94.7(4.0)\ \text{MeV}. \tag{C.12}$$

These numbers should be confronted with the values quoted in [51] and [53].

JHEP11(2018)032

C.1.2 Decay constant of η_c meson

The decay constant of η_c meson is defined as [102]

$$\langle 0|\,\bar{c}\gamma^\mu\gamma^5 c\,|\eta_c\rangle \equiv i f_{\eta_c}^{\rm exp} p^\mu, \tag{C.13}$$

where $f_{\eta_c}^{\rm exp} = 335\,\text{MeV}$, as measured by CLEO collaboration [103]. Our definition (B.32) differs by factor $\sqrt{2}$, so $f_{\eta_c} = f_{\eta_c}^{\rm exp}/\sqrt{2} \approx 237\,\text{MeV}$.

C.1.3 Decay constant of ρ meson

There are 2 parametrizations of the ρ charged current matrix element using g_ρ, defined by (B.34), or f_ρ, which is related to g_ρ are $f_\rho = g_\rho/m_\rho$. The value of the decay constant can be obtained by 2 methods: from $\rho \to e^+e^-$ using approximate symmetry (B.27) or from the τ-lepton decay. Results, obtained in ref. [95] by these two method differ by about 5%, $f_{\rho,ee} = 220(2)\,\text{MeV}$ and $f_{\rho,\tau} = 209(4)\,\text{MeV}$. We calculate

$$\Gamma(\tau \to \nu\rho) = \frac{G_F^2 g_\rho^2 m_\tau^3}{16\pi m_\rho^2}|V_{ud}|^2 \left(1 + 2\frac{m_\rho^2}{m_\tau^2}\right)\left(1 - \frac{m_\rho^2}{m_\tau^2}\right)^2, \tag{C.14}$$

$$\Gamma(\rho \to e^+e^-) = \frac{e^4 g_\rho^2}{24\pi m_\rho^3}, \tag{C.15}$$

and get $g_{\rho,\tau} = 0.162\,\text{GeV}^2$ and $g_{\rho,ee} = 0.171\,\text{GeV}^2$, which corresponds to $f_{\rho,\tau} = 209\,\text{MeV}$ and $f_{\rho,ee} = 221\,\text{MeV}$ in full agreement with [95]. The difference between these results can be explained by the approximaty of the relation (B.27). So we use $g_{\rho,\tau}$ value as more directly measured one. The results of our analysis agrees with f_ρ value in [53] (within about 10%), but differ from the value adopted in [51] by $\sim 25\%$.

C.2 Meson form factors of decay into pseudoscalar meson

To describe the semileptonic decays of the pseudoscalar meson into another pseudoscalar meson one should know the form factors $f_+(q^2)$, $f_0(q^2)$, $f_-(q^2)$ defined by eq. (A.13), only two of which are independent. We use $f_+(q^2)$, $f_0(q^2)$ pair for the decay parametrization.

In turn, there are many different parametrizations of meson form factors. One popular parametrization is the Bourrely-Caprini-Lellouch (BCL) parametrization [104] that takes into account the analytic properties of form factors (see e.g. [105, 106]),

$$f(q^2) = \frac{1}{1 - q^2/M_{\rm pole}^2}\sum_{n=0}^{N-1} a_n\left[\big(z(q^2)\big)^n - (-1)^{n-N}\frac{n}{N}\big(z(q^2)\big)^N\right] \tag{C.16}$$

where the function $z(q^2)$ is defined via

$$z(q^2) \equiv \frac{\sqrt{t_+ - q^2} - \sqrt{t_+ - t_0}}{\sqrt{t_+ - q^2} + \sqrt{t_+ - t_0}} \tag{C.17}$$

with

$$t_+ = \big(m_h + m_{h'}\big)^2. \tag{C.18}$$

JHEP11(2018)032

h, h'	$f_{+,0}(0)$	λ_+	λ_0
K^0, π^+	0.970	0.0267	0.0117
K^+, π^0	0.970	0.0277	0.0183

Table 10. Best fit parameters for the form factors (C.20) of $D \to \pi$ and $D \to K$ transitions [106–108].

f	$f(0)$	c	P (GeV^{-2})
f_+^{DK}	0.7647	0.066	0.224
f_0^{DK}	0.7647	2.084	0
$f_+^{D\pi}$	0.6117	1.985	0.1314
$f_0^{D\pi}$	0.6117	1.188	0.0342

Table 11. Best fit parameters for the form factors (C.21) of $D \to \pi$ and $D \to K$ transitions [109].

The choice of t_0 and of the pole mass M_{pole} varies from group to group that performs the analysis. In this work we follow FLAG collaboration [106] and take

$$t_0 = \left(m_h + m_{h'}\right)\left(\sqrt{m_h} - \sqrt{m_{h'}}\right)^2. \tag{C.19}$$

The coefficients a_n^+ and a_n^0 are then fitted to the experimental data or lattice results.

C.2.1 K meson form factors

Form factors of $K \to \pi$ transition are well described by the linear approximation [107, 108]

$$f_{+,0}^{K\pi}(q^2) = f_{+,0}^{K\pi}(0)\left(1 + \lambda_{+,0}\frac{q^2}{m_{\pi^+}^2}\right). \tag{C.20}$$

The best fit parameters are given in table 10.

C.2.2 D meson form factors

In the recent paper [109] the form factors for $D \to K$ and $D \to \pi$ transitions are given in the form

$$f(q^2) = \frac{f(0) - c(z(q^2) - z_0)\left(1 + \frac{z(q^2)+z_0}{2}\right)}{1 - Pq^2}, \tag{C.21}$$

where $z_0 = z(0)$. The best fit parameter values are given in table 11.

Form factors of $D_s \to \eta$ transition read [110]

$$f_+^{D_s\eta}(q^2) = \frac{f_+^{D_s\eta}(0)}{\left(1 - q^2/m_{D_s^*}^2\right)\left(1 - \alpha_+^{D_s\eta} q^2/m_{D_s^*}^2\right)}, \tag{C.22}$$

$$f_0^{D_s\eta}(q^2) = \frac{f_0^{D_s\eta}(0)}{1 - \alpha_0^{D_s\eta} q^2/m_{D_s^*}^2}, \tag{C.23}$$

where $f_+^{D_s\eta}(0) = 0.495$, $\alpha_+^{D_s\eta} = 0.198$ [110], $m_{D_s^*} = 2.112\,\text{GeV}$ [65]. Scalar form factor $f_0^{D_s\eta}(q^2)$ is not well constrained by experimental data, so we take $f_0^{D_s\eta}(q^2) = f_+^{D_s\eta}(q^2)$ by eq. (A.14) and $\alpha_0^{D_s\eta} = 0$.

JHEP11(2018)032

f	M_{pole} (GeV)	a_0	a_1	a_2
$f_+^{B_{(s)}D_{(s)}}$	∞	0.909	−7.11	66
$f_0^{B_{(s)}D_{(s)}}$	∞	0.794	−2.45	33
$f_+^{B_sK}$	$m_{B^*} = 5.325$	0.360	−0.828	1.1
$f_0^{B_sK}$	$m_{B^*(0^+)} = 5.65$	0.233	0.197	0.18
$f_+^{B\pi}$	$m_{B^*} = 5.325$	0.404	−0.68	−0.86
$f_0^{B\pi}$	$m_{B^*(0^+)} = 5.65$	0.490	−1.61	0.93

Table 12. Best fit parameters for the form factors (C.16) of $B \to \pi$, $B_{(s)} \to D_{(s)}$ and $B_s \to K$ transitions [106].

C.2.3 B meson form factors

Most of B meson form factors are available in literature in the form (C.16), their best fit parameter values are given in table 12. The form factors for $B_s \to D_s$ are almost the same as for $B \to D$ transition [111], so we use the same expressions for both cases.

C.3 Meson form factors for decay into vector meson

One of the relevant HNL production channel is pseudoscalar meson decay $h_P \to h'_V \ell_\alpha N$. To compute decay width of this decay one needs to know the form factors $g(q^2)$, $f(q^2)$, $a_\pm(q^2)$, defined by eqs. (A.15), (A.16). The dimensionless linear combinations are introduced as

$$V^{hh'}(q^2) = (m_h + m_{h'})\, g^{hh'}(q^2), \tag{C.24}$$

$$A_0^{hh'}(q^2) = \frac{1}{2m_{h'}} \left(f^{hh'}(q^2) + q^2 a_-^{hh'}(q^2) + \left(m_h^2 - m_{h'}^2\right) a_+^{hh'}(q^2) \right), \tag{C.25}$$

$$A_1^{hh'}(q^2) = \frac{f^{hh'}(q^2)}{m_h + m_{h'}}, \tag{C.26}$$

$$A_2^{hh'}(q^2) = -\left(m_h + m_{h'}\right) a_+^{hh'}(q^2). \tag{C.27}$$

For these linear combinations the following ansatz is used

$$V^{hh'}(q^2) = \frac{f_V^{hh'}}{\left(1 - q^2/(M_V^h)^2\right)\left[1 - \sigma_V^{hh'} q^2/(M_V^h)^2 - \xi_V^{hh'} q^4/(M_V^h)^4\right]}, \tag{C.28}$$

$$A_0^{hh'}(q^2) = \frac{f_{A_0}^{hh'}}{\left(1 - q^2/(M_P^h)^2\right)\left[1 - \sigma_{A_0}^{hh'} q^2/(M_V^h)^2 - \xi_{A_0}^{hh'} q^4/(M_V^h)^4\right]}, \tag{C.29}$$

$$A_{1/2}^{hh'}(q^2) = \frac{f_{A_{1/2}}^{hh'}}{1 - \sigma_{A_{1/2}}^{hh'} q^2/(M_V^h)^2 - \xi_{A_{1/2}}^{hh'} q^4/(M_V^h)^4}. \tag{C.30}$$

Best fit values of parameters are adopted from papers [112–114]. f, σ parameters are given in table 13, while ξ and the pole masses M_V and M_P are given in table 14.

JHEP11(2018)032

h, h'	$f_V^{hh'}$	$f_{A_0}^{hh'}$	$f_{A_1}^{hh'}$	$f_{A_2}^{hh'}$	$\sigma_V^{hh'}$	$\sigma_{A_0}^{hh'}$	$\sigma_{A_1}^{hh'}$	$\sigma_{A_2}^{hh'}$
D, K^*	1.03	0.76	0.66	0.49	0.27	0.17	0.30	0.67
B, D^*	0.76	0.69	0.66	0.62	0.57	0.59	0.78	1.40
B, ρ	0.295	0.231	0.269	0.282	0.875	0.796	0.54	1.34
B_s, D_s^*	0.95	0.67	0.70	0.75	0.372	0.350	0.463	1.04
B_s, K^*	0.291	0.289	0.287	0.286	−0.516	−0.383	0	1.05

Table 13. First part of the table with parameters of meson form factors (C.28)–(C.30) of decay into vector meson [112–114].

h, h'	$\xi_V^{hh'}$	$\xi_{A_0}^{hh'}$	$\xi_{A_1}^{hh'}$	$\xi_{A_2}^{hh'}$	M_P^h (GeV)	M_V^h (GeV)
D, K^*	0	0	0.20	0.16	$m_{D_s} = 1.969$	$m_{D_s^*} = 2.112$
B, D^*	0	0	0	0.41	$m_{B_c} = 6.275$	$m_{B_c^*} = 6.331$
B, ρ	0	0.055	0	−0.21	$m_B = 5.279$	$m_{B^*} = 5.325$
B_s, D_s^*	0.561	0.600	0.510	0.070	$m_{B_c} = 6.275$	$m_{B_c^*} = 6.331$
B_s, K^*	2.10	1.58	1.06	−0.074	$m_{B_s} = 5.367$	$m_{B_s^*} = 5.415$

Table 14. Second part of the table with parameters of meson form factors (C.28)–(C.30) of decay into vector meson [112–114]. Masses of B_c, D_s and D_s^* are taken from [65], while for B_c^* theoretical prediction [115] is used.

D Production from J/ψ and Υ mesons

D.1 Production from J/ψ

The process $J/\psi \to N\bar{\nu}$ allows to creates HNLs with mass up to $M_{J/\psi} \simeq 3.1$ GeV and therefore contribute to the production *above* the D-meson threshold.

To estimate $\mathrm{BR}(J/\psi \to N\bar{\nu})$ let us first compare the processes $J/\psi \to e^+e^-$ and $J/\psi \to \nu_e\bar{\nu}_e$. The ratio of their width is given by [116]

$$\frac{\mathrm{BR}(J/\psi \to \nu_e\bar{\nu}_e)}{\mathrm{BR}(J/\psi \to e^+e^-)} = \frac{27 G_F^2 M_{J/\psi}^4}{256\pi^2\alpha^2}\left(1 - \frac{8}{3}\sin^2\theta_W\right)^2 \sim 4.5 \times 10^{-7} \tag{D.1}$$

with the precision of the order of few per cent [116]. Using the measured branching ratio $\mathrm{BR}(J/\psi \to e^+e^-) \simeq 0.06$ [65], one can estimate decay into *one flavour of neutrinos*, $\mathrm{BR}(J/\psi \to \nu_e\bar{\nu}_e) \simeq 2.7\times10^{-8}$. The corresponding branching of J/ψ to HNL is additionally suppressed by U^2 and by the phase-space factor f_{PS}:

$$\sum_\alpha \mathrm{BR}(J/\psi \to N\bar{\nu}_\alpha) = U^2 f_{PS}(M_N/M_{J/\psi})\,\mathrm{BR}(J/\psi \to \nu_e\bar{\nu}_e) \tag{D.2}$$

We estimate this fraction at $M_N = M_D$ (just above the D-meson threshold) taking for simplicity $f_{PS} = 1$. Clearly, at masses below M_D the production from D-mesons dominates (as the J/ψ production fraction $f(J/\psi) \simeq 0.01$, see [5, Appendix A], reproduced

JHEP11(2018)032

for completeness in appendix E). Above D-meson mass but below $M_{J/\psi}$ we should compare with the production from B mesons. We compare the probability to produce HNL from B-meson and from J/ψ:

$$\frac{\text{HNLs from } J/\psi}{\text{HNLs from } B} = \frac{X_{c\bar{c}} \times f(J/\psi) \times \text{BR}_{J/\psi \to N\bar{\nu}}}{X_{b\bar{b}} \times f(B) \times \text{BR}_{B\to NX}} = 3 \times 10^{-4} \left(\frac{X_{c\bar{c}}}{10^{-3}}\right) \left(\frac{10^{-7}}{X_{b\bar{b}}}\right) \tag{D.3}$$

where we have adopted $f(B) \times BR(B \to N + X) \sim 10^{-2}$ (cf. figure 4, right panel) and used $f(J/\psi) \sim 10^{-2}$. The numbers in (2.4) are normalized to SHiP. We see therefore that J/ψ decays contribute sub-dominantly while $X_{b\bar{b}}/X_{c\bar{c}} \gtrsim 10^{-8}$.

D.2 Production from Υ

The heavy mass of Υ opens up a possibility to produce HNLs up to $M_N \simeq 10$GeV. Similarly to eq. (D.1) we can find the branching ratio $\text{BR}(\Upsilon \to \nu\bar{\nu}) = 4 \times 10^{-4}\,\text{BR}(\Upsilon \to e^+e^-)$ [116]. Therefore

$$\text{BR}(\Upsilon \to N\bar{\nu}_\alpha) = U_\alpha^2 f_{PS}(M_N/M_\Upsilon) \frac{27 G_F^2 M_\Upsilon^4}{64\pi^2\alpha^2} \left(-1 + \frac{4}{3}\sin^2\theta_W\right)^2 \text{BR}(\Upsilon \to e^+e^-) \tag{D.4}$$

Using the latest measurement $\text{BR}(\Upsilon \to e^+e^-) \simeq 2.4 \times 10^{-2}$ [65] one finds that $\text{BR}(\Upsilon \to \nu\bar{\nu}) \simeq 10^{-5}$. We do not know the fraction $f(\Upsilon)$ out of all $b\bar{b}$ pairs, but one can roughly estimate it equal to the fraction $f(J/\psi) \sim 1\%$ (see appendix E in [5]), so

$$N_{\Upsilon \to N\bar{\nu}} \simeq 10^{-10} N_\Upsilon \times \left(\frac{U^2}{10^{-5}}\right) \tag{D.5}$$

where we have normalized U^2 to the current experimental limit for $M_N > 5\,\text{GeV}$ (cf. figure 1).

E Production of heavy flavour at SHiP

For a particular application of the obtained results we revise the HNL production at the SHiP experiment. The number of mesons produced by $E_p = 400\,\text{GeV}$ proton beam at the SHiP target can be estimated as

$$N_h = 2 \times f(h) \times X_{q\bar{q}} \times N_{\text{PoT}} \tag{E.1}$$

where $X_{q\bar{q}}$ represents the $q\bar{q}$ production rate, $f(h)$ is the meson h production fraction[11] and expected number of protons on target is $N_{\text{PoT}} = 2 \cdot 10^{20}$. The following cross sections have been used for the estimates:

- the proton-nucleon cross section is $\sigma(pN) \simeq 10.7$ mbarn.
- $X_{ss} \approx 1/7$ [51].
- $\sigma(cc) = 18$ μbarn [117] and the fraction $X_{cc} = 1.7 \times 10^{-3}$
- $\sigma(bb) = 1.7$ nbarn [118] and the fraction $X_{bb} = 1.6 \times 10^{-7}$

[11] $f(h)$ is equal to the number of h mesons divided by the number of corresponding quarks.

JHEP11(2018)032

Meson	$f(h)$	N_h
K	–	$5.7 \cdot 10^{19}$
$D^{\pm}$	0.207	$1.4 \cdot 10^{17}$
D^0	0.632	$4.3 \cdot 10^{17}$
D_s	0.088	$6.0 \cdot 10^{16}$
J/ψ	0.01	$6.8 \cdot 10^{15}$
$B^{\pm}$	0.417	$2.7 \cdot 10^{13}$
B^0	0.418	$2.7 \cdot 10^{13}$
B_s	0.113	$7.2 \cdot 10^{12}$

Table 15. Production fraction and expected number of different mesons in SHiP.

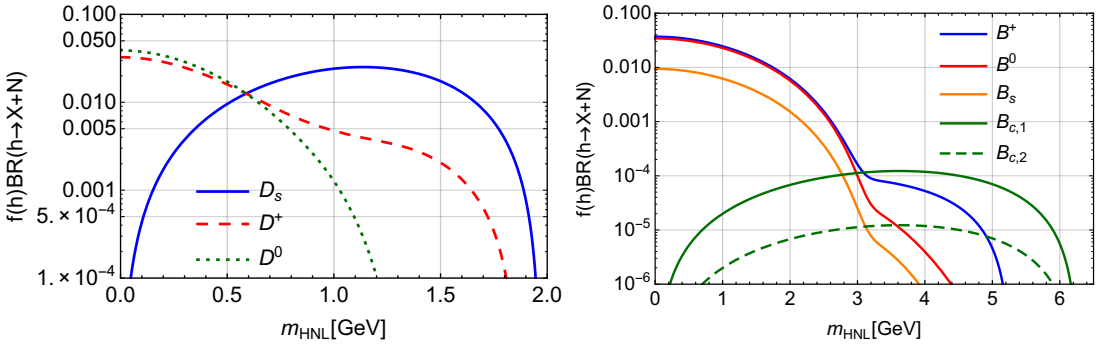

Figure 21. Branching ratio × Production fraction for charm to HNL (left panel) and for beauty to HNL (right panel) for SHiP experiment and mixing angles $U_e = 1$, $U_\mu = U_\tau = 0$. For B_c meson $f(B_c)$ is unknown, so the result is shown for two values, $f(B_c) = 2 \cdot 10^{-3}$ ($B_{c,1}$ line) and $f(B_c) = 2 \cdot 10^{-4}$ ($B_{c,2}$ line).

To calculate the meson production fractions the dedicated simulation is needed. It should take into account the properties of the target (materials, geometry) and the cascade processes (birth of the excited meson states like D^* and its decay into D). The values of $f(h)$ for the case of SHiP were calculated in the paper [57]. These values with the number of different mesons are presented in table 15. For kaons we do not divide them for species. Taking into account production fractions of different mesons the main production channels from charm and beauty quarks for SHiP are shown in figure 21.

The expected number of τ-leptons for $N_{\rm PoT} = 2 \times 10^{20}$ is $N_\tau = 3 \times 10^{15}$.

F Vector-dominance model

Here we provide $F_\pi(s)$ formula, given by vector-dominance model [87]

$$F_\pi(s) = \frac{\mathrm{BW}_\rho^{\rm GS}(s)\frac{1+c_\omega \mathrm{BW}_\omega^{\rm KS}(s)}{1+c_\omega} + c_{\rho'}\mathrm{BW}_{\rho'}^{\rm GS}(s) + c_{\rho''}\mathrm{BW}_{\rho''}^{\rm GS}(s) + c_{\rho'''}\mathrm{BW}_{\rho'''}^{\rm GS}(s)}{1 + c_{\rho'} + c_{\rho''} + c_{\rho'''}}, \qquad \text{(F.1)}$$

where $c_i = |c_i|e^{i\phi_i}$ are complex amplitudes of the Breit-Wigner (BW) functions. They are different for ω and ρ mesons. For ω it is the usual BW function

$$\mathrm{BW}_\omega^{\rm KS}(s) = \frac{m_\omega^2}{m_\omega^2 - s - i m_\omega \Gamma_\omega}, \qquad \text{(F.2)}$$

JHEP11(2018)032

while for ρ mesons Gounaris-Sakurai (GS) model [119] is taken,

$$\mathrm{BW}^{\mathrm{GS}}_{\rho_i}(s) = \frac{m^2_{\rho_i}(1 + d(m_{\rho_i})\Gamma_{\rho_i}/m_{\rho_i})}{m^2_{\rho_i} - s + f(s, m_{\rho_i}, \Gamma_{\rho_i}) - i m_{\rho_i}\Gamma(s, m_{\rho_i}, \Gamma_{\rho_i})}, \tag{F.3}$$

where

$$\Gamma(s, m, \Gamma) = \Gamma \frac{s}{m^2}\left(\frac{\beta_\pi(s)}{\beta_\pi(m^2)}\right)^3, \tag{F.4}$$

$$f(s, m, \Gamma) = \frac{\Gamma m^2}{k^3(m^2)}\left[k^2(s)\left(h(s) - h(m^2)\right) + (m^2 - s)k^2(m^2)h'(m^2)\right] \tag{F.5}$$

$$\beta_\pi(s) = \sqrt{1 - \frac{4m^2_\pi}{s}}, \tag{F.6}$$

$$d(m) = \frac{3}{\pi}\frac{m^2_\pi}{k^2(m^2)}\ln\left(\frac{m^2 + 2k(m^2)}{2m_\pi}\right) + \frac{m}{2\pi k(m^2)} - \frac{m^2_\pi m}{\pi k^3(m^2)}, \tag{F.7}$$

$$k(s) = \frac{1}{2}\sqrt{s}\beta_\pi(s), \tag{F.8}$$

$$h(s) = \frac{2}{\pi}\frac{k(s)}{\sqrt{s}}\ln\left(\frac{\sqrt{s} + 2k(s)}{2m_\pi}\right) \tag{F.9}$$

and $h'(s)$ is a derivative of $h(s)$.

References

[1] T. Asaka, S. Blanchet and M. Shaposhnikov, *The nuMSM, dark matter and neutrino masses*, *Phys. Lett.* **B 631** (2005) 151 [hep-ph/0503065] [INSPIRE].

[2] T. Asaka and M. Shaposhnikov, *The nuMSM, dark matter and baryon asymmetry of the universe*, *Phys. Lett.* **B 620** (2005) 17 [hep-ph/0505013] [INSPIRE].

[3] A. Boyarsky, O. Ruchayskiy and M. Shaposhnikov, *The role of sterile neutrinos in cosmology and astrophysics*, *Ann. Rev. Nucl. Part. Sci.* **59** (2009) 191 [arXiv:0901.0011] [INSPIRE].

[4] M. Drewes, *The phenomenology of right handed neutrinos*, *Int. J. Mod. Phys.* **E 22** (2013) 1330019 [arXiv:1303.6912] [INSPIRE].

[5] S. Alekhin et al., *A facility to search for hidden particles at the CERN SPS: the SHiP physics case*, *Rept. Prog. Phys.* **79** (2016) 124201 [arXiv:1504.04855] [INSPIRE].

[6] LBNE collaboration, C. Adams et al., *The long-baseline neutrino experiment: exploring fundamental symmetries of the universe*, arXiv:1307.7335 [INSPIRE].

[7] SHiP collaboration, P. Mermod, *Prospects of the SHiP and NA62 experiments at CERN for hidden sector searches*, *PoS* **NuFact2017** (2017) 139 [arXiv:1712.01768] [INSPIRE].

[8] NA62 collaboration, E. Cortina Gil et al., *Search for heavy neutral lepton production in K^+ decays*, *Phys. Lett.* **B 778** (2018) 137 [arXiv:1712.00297] [INSPIRE].

JHEP11(2018)032

[9] M. Drewes, J. Hajer, J. Klaric and G. Lanfranchi, *NA62 sensitivity to heavy neutral leptons in the low scale seesaw model*, *JHEP* **07** (2018) 105 [arXiv:1801.04207] [INSPIRE].

[10] SHiP collaboration, M. Anelli et al., *A facility to Search for Hidden Particles (SHiP) at the CERN SPS*, arXiv:1504.04956 [INSPIRE].

[11] V.V. Gligorov, S. Knapen, M. Papucci and D.J. Robinson, *Searching for Long-lived Particles: A Compact Detector for Exotics at LHCb*, *Phys. Rev.* **D 97** (2018) 015023 [arXiv:1708.09395] [INSPIRE].

[12] J.P. Chou, D. Curtin and H.J. Lubatti, *New detectors to explore the lifetime frontier*, *Phys. Lett.* **B 767** (2017) 29 [arXiv:1606.06298] [INSPIRE].

[13] D. Curtin and M.E. Peskin, *Analysis of long lived particle decays with the MATHUSLA detector*, *Phys. Rev.* **D 97** (2018) 015006 [arXiv:1705.06327] [INSPIRE].

[14] J.A. Evans, *Detecting hidden particles with MATHUSLA*, *Phys. Rev.* **D 97** (2018) 055046 [arXiv:1708.08503] [INSPIRE].

[15] J.C. Helo, M. Hirsch and Z.S. Wang, *Heavy neutral fermions at the high-luminosity LHC*, *JHEP* **07** (2018) 056 [arXiv:1803.02212] [INSPIRE].

[16] J.L. Feng, I. Galon, F. Kling and S. Trojanowski, *ForwArd Search ExpeRiment at the LHC*, *Phys. Rev.* **D 97** (2018) 035001 [arXiv:1708.09389] [INSPIRE].

[17] J.L. Feng, I. Galon, F. Kling and S. Trojanowski, *Dark Higgs bosons at the ForwArd Search ExpeRiment*, *Phys. Rev.* **D 97** (2018) 055034 [arXiv:1710.09387] [INSPIRE].

[18] F. Kling and S. Trojanowski, *Heavy neutral leptons at FASER*, *Phys. Rev.* **D 97** (2018) 095016 [arXiv:1801.08947] [INSPIRE].

[19] Belle collaboration, D. Liventsev et al., *Search for heavy neutrinos at Belle*, *Phys. Rev.* **D 87** (2013) 071102 [*Erratum ibid.* **D 95** (2017) 099903] [arXiv:1301.1105] [INSPIRE].

[20] LHCb collaboration, *Search for Majorana neutrinos in $B^- \to \pi^+\mu^-\mu^-$ decays*, *Phys. Rev. Lett.* **112** (2014) 131802 [arXiv:1401.5361] [INSPIRE].

[21] CMS collaboration, *Search for heavy Majorana neutrinos in $\mu^\pm\mu^\pm$+ jets events in proton-proton collisions at $\sqrt{s}$ = 8 TeV*, *Phys. Lett.* **B 748** (2015) 144 [arXiv:1501.05566] [INSPIRE].

[22] ATLAS collaboration, *Search for heavy Majorana neutrinos with the ATLAS detector in pp collisions at $\sqrt{s} = 8$ TeV*, *JHEP* **07** (2015) 162 [arXiv:1506.06020] [INSPIRE].

[23] CMS collaboration, *Search for heavy neutral leptons in events with three charged leptons in proton-proton collisions at $\sqrt{s} = 13$ TeV*, *Phys. Rev. Lett.* **120** (2018) 221801 [arXiv:1802.02965] [INSPIRE].

[24] A. Izmaylov and S. Suvorov, *Search for heavy neutrinos in the ND280 near detector of the T2K experiment*, *Phys. Part. Nucl.* **48** (2017) 984.

[25] T. Asaka, S. Eijima and A. Watanabe, *Heavy neutrino search in accelerator-based experiments*, *JHEP* **03** (2013) 125 [arXiv:1212.1062] [INSPIRE].

[26] T. Asaka and S. Eijima, *Direct search for right-handed neutrinos and neutrinoless double beta decay*, *PTEP* **2013** (2013) 113B02 [arXiv:1308.3550] [INSPIRE].

[27] FCC-ee study Team collaboration, A. Blondel et al., *Search for heavy right handed neutrinos at the FCC-ee*, *Nucl. Part. Phys. Proc.* **273-275** (2016) 1883 [arXiv:1411.5230] [INSPIRE].

[28] T. Asaka, S. Eijima and K. Takeda, *Lepton universality in the νMSM*, *Phys. Lett.* **B 742** (2015) 303 [arXiv:1410.0432] [INSPIRE].

JHEP11(2018)032

[29] L. Canetti, M. Drewes and B. Garbrecht, *Probing leptogenesis with GeV-scale sterile neutrinos at LHCb and Belle II*, *Phys. Rev.* **D 90** (2014) 125005 [arXiv:1404.7114] [INSPIRE].

[30] A. Das, P.S. Bhupal Dev and N. Okada, *Direct bounds on electroweak scale pseudo-Dirac neutrinos from $\sqrt{s} = 8$ TeV LHC data*, *Phys. Lett.* **B 735** (2014) 364 [arXiv:1405.0177] [INSPIRE].

[31] A.M. Gago et al., *Probing the type I seesaw mechanism with displaced vertices at the LHC*, *Eur. Phys. J.* **C 75** (2015) 470 [arXiv:1505.05880] [INSPIRE].

[32] S. Antusch and O. Fischer, *Testing sterile neutrino extensions of the standard model at future lepton colliders*, *JHEP* **05** (2015) 053 [arXiv:1502.05915] [INSPIRE].

[33] A. Das and N. Okada, *Improved bounds on the heavy neutrino productions at the LHC*, *Phys. Rev.* **D 93** (2016) 033003 [arXiv:1510.04790] [INSPIRE].

[34] T. Asaka and A. Watanabe, *Probing heavy neutrinos in the COMET experiment*, *PTEP* **2016** (2016) 033B03 [arXiv:1510.07746] [INSPIRE].

[35] T. Asaka and T. Tsuyuki, *Seesaw mechanism at electron-electron colliders*, *Phys. Rev.* **D 92** (2015) 094012 [arXiv:1508.04937] [INSPIRE].

[36] T. Asaka and H. Ishida, *Lepton number violation by heavy Majorana neutrino in B decays*, *Phys. Lett.* **B 763** (2016) 393 [arXiv:1609.06113] [INSPIRE].

[37] G. Cvetič and C.S. Kim, *Rare decays of B mesons via on-shell sterile neutrinos*, *Phys. Rev.* **D 94** (2016) 053001 [*Erratum ibid.* **D 95** (2017) 039901] [arXiv:1606.04140] [INSPIRE].

[38] A. Caputo et al., *The seesaw path to leptonic CP-violation*, *Eur. Phys. J.* **C 77** (2017) 258 [arXiv:1611.05000] [INSPIRE].

[39] R.W. Rasmussen and W. Winter, *Perspectives for tests of neutrino mass generation at the GeV scale: experimental reach versus theoretical predictions*, *Phys. Rev.* **D 94** (2016) 073004 [arXiv:1607.07880] [INSPIRE].

[40] A. Das, P.S.B. Dev and C.S. Kim, *Constraining sterile neutrinos from precision Higgs data*, *Phys. Rev.* **D 95** (2017) 115013 [arXiv:1704.00880] [INSPIRE].

[41] S. Antusch, E. Cazzato and O. Fischer, *Sterile neutrino searches via displaced vertices at LHCb*, *Phys. Lett.* **B 774** (2017) 114 [arXiv:1706.05990] [INSPIRE].

[42] A. Caputo, P. Hernández, J. Lopez-Pavon and J. Salvado, *The seesaw portal in testable models of neutrino masses*, *JHEP* **06** (2017) 112 [arXiv:1704.08721] [INSPIRE].

[43] A. Das, Y. Gao and T. Kamon, *Heavy neutrino search via the Higgs boson at the LHC*, arXiv:1704.00881 [INSPIRE].

[44] E.J. Chun et al., *Probing leptogenesis*, *Int. J. Mod. Phys.* **A 33** (2018) 1842005 [arXiv:1711.02865] [INSPIRE].

[45] C.-X. Yue, Y.-C. Guo and Z.-H. Zhao, *Majorana neutrino signals at Belle-II and ILC*, *Nucl. Phys.* **B 925** (2017) 186 [arXiv:1710.06144] [INSPIRE].

[46] S. Antusch et al., *Probing leptogenesis at future colliders*, *JHEP* **09** (2018) 124 [arXiv:1710.03744] [INSPIRE].

[47] A. Das, *Searching for the minimal Seesaw models at the LHC and beyond*, *Adv. High Energy Phys.* **2018** (2018) 9785318 [arXiv:1803.10940] [INSPIRE].

[48] G. Cvetič, A. Das and J. Zamora-Saá, *Probing heavy neutrino oscillations in rare W boson decays*, arXiv:1805.00070 [INSPIRE].

JHEP11(2018)032

[49] L.M. Johnson, D.W. McKay and T. Bolton, *Extending sensitivity for low mass neutral heavy lepton searches*, *Phys. Rev.* **D 56** (1997) 2970 [hep-ph/9703333] [INSPIRE].

[50] V. Gribanov, S. Kovalenko and I. Schmidt, *Sterile neutrinos in tau lepton decays*, *Nucl. Phys.* **B 607** (2001) 355 [hep-ph/0102155] [INSPIRE].

[51] D. Gorbunov and M. Shaposhnikov, *How to find neutral leptons of the νMSM?*, *JHEP* **10** (2007) 015 [*Erratum ibid.* **1311** (2013) 101] [arXiv:0705.1729] [INSPIRE].

[52] S. Ramazanov, *Semileptonic decays of charmed and beauty baryons with sterile neutrinos in the final state*, *Phys. Rev.* **D 79** (2009) 077701 [arXiv:0810.0660] [INSPIRE].

[53] A. Atre, T. Han, S. Pascoli and B. Zhang, *The search for heavy Majorana neutrinos*, *JHEP* **05** (2009) 030 [arXiv:0901.3589] [INSPIRE].

[54] J.C. Helo, S. Kovalenko and I. Schmidt, *Sterile neutrinos in lepton number and lepton flavor violating decays*, *Nucl. Phys.* **B 853** (2011) 80 [arXiv:1005.1607] [INSPIRE].

[55] A. Abada, A.M. Teixeira, A. Vicente and C. Weiland, *Sterile neutrinos in leptonic and semileptonic decays*, *JHEP* **02** (2014) 091 [arXiv:1311.2830] [INSPIRE].

[56] J.C. Helo, M. Hirsch and S. Kovalenko, *Heavy neutrino searches at the LHC with displaced vertices*, *Phys. Rev.* **D 89** (2014) 073005 [*Erratum ibid.* **D 93** (2016) 099902] [arXiv:1312.2900] [INSPIRE].

[57] E. Graverini, E. van Herwijnen and T. Ruf, *Mass dependence of branching ratios into HNL for FairShip*, CERN-SHiP-NOTE-2016-001 (2016).

[58] G. Anamiati, R.M. Fonseca and M. Hirsch, *Quasi Dirac neutrino oscillations*, *Phys. Rev.* **D 97** (2018) 095008 [arXiv:1710.06249] [INSPIRE].

[59] S. Antusch, E. Cazzato and O. Fischer, *Heavy neutrino-antineutrino oscillations at colliders*, arXiv:1709.03797 [INSPIRE].

[60] SHiP collaboration, *Sensitivity of the SHiP experiment to Heavy Neutral Leptons*, to appear (2018).

[61] K. Bondarenko, A. Boyarsky, M. Ovchynnikov and O. Ruchayskiy, *Sensitivity of the intensity frontier experiments for neutrino and scalar portals: analytic estimates*, to appear (2018).

[62] A.D. Dolgov, S.H. Hansen, G. Raffelt and D.V. Semikoz, *Heavy sterile neutrinos: Bounds from big bang nucleosynthesis and SN1987A*, *Nucl. Phys.* **B 590** (2000) 562 [hep-ph/0008138] [INSPIRE].

[63] R.E. Shrock, *General theory of weak leptonic and semileptonic decays. 1. Leptonic pseudoscalar meson decays, with associated tests for and bounds on, neutrino masses and lepton mixing*, *Phys. Rev.* **D 24** (1981) 1232 [INSPIRE].

[64] R.E. Shrock, *New tests for, and bounds on, neutrino masses and lepton mixing*, *Phys. Lett.* **B 96** (1980) 159.

[65] Particle Data Group collaboration, C. Patrignani et al., *Review of particle physics*, *Chin. Phys.* **C40** (2016) 100001.

[66] LHCb collaboration, *Observation of $B_c^+ \to D^0 K^+$ decays*, *Phys. Rev. Lett.* **118** (2017) 111803 [arXiv:1701.01856] [INSPIRE].

[67] J. Mejia-Guisao, D. Milanes, N. Quintero and J.D. Ruiz-Alvarez, *Exploring GeV-scale Majorana neutrinos in lepton-number-violating Λ_b^0 baryon decays*, *Phys. Rev.* **D 96** (2017) 015039 [arXiv:1705.10606] [INSPIRE].

JHEP11(2018)032

[68] H.-Y. Cheng and B. Tseng, $1/M$ *corrections to baryonic form-factors in the quark model*, *Phys. Rev.* **D 53** (1996) 1457 [*Erratum ibid.* **D 55** (1997) 1697] [hep-ph/9502391] [INSPIRE].

[69] S. Meinel, $\Lambda_c \to \Lambda l^+ \nu_l$ *form factors and decay rates from lattice QCD with physical quark masses*, *Phys. Rev. Lett.* **118** (2017) 082001 [arXiv:1611.09696] [INSPIRE].

[70] W. Detmold, C. Lehner and S. Meinel, $\Lambda_b \to p\ell^-\bar{\nu}_\ell$ *and* $\Lambda_b \to \Lambda_c\ell^-\bar{\nu}_\ell$ *form factors from lattice QCD with relativistic heavy quarks*, *Phys. Rev.* **D 92** (2015) 034503 [arXiv:1503.01421] [INSPIRE].

[71] G. Källén, *Elementary particle physics*, Addison-Wesley series in advanced physics, Addison-Wesley Pub. Co., U.S.A. (1964).

[72] C. Degrande, O. Mattelaer, R. Ruiz and J. Turner, *Fully-automated precision predictions for heavy neutrino production mechanisms at hadron colliders*, *Phys. Rev.* **D 94** (2016) 053002 [arXiv:1602.06957] [INSPIRE].

[73] R. Ruiz, M. Spannowsky and P. Waite, *Heavy neutrinos from gluon fusion*, *Phys. Rev.* **D 96** (2017) 055042 [arXiv:1706.02298] [INSPIRE].

[74] A. Pilaftsis, *Radiatively induced neutrino masses and large Higgs neutrino couplings in the standard model with Majorana fields*, *Z. Phys.* **C 55** (1992) 275 [hep-ph/9901206] [INSPIRE].

[75] A. Datta, M. Guchait and A. Pilaftsis, *Probing lepton number violation via Majorana neutrinos at hadron supercolliders*, *Phys. Rev.* **D 50** (1994) 3195 [hep-ph/9311257] [INSPIRE].

[76] A. Buckley et al., *LHAPDF6: parton density access in the LHC precision era*, *Eur. Phys. J.* **C 75** (2015) 132 [arXiv:1412.7420] [INSPIRE].

[77] H.-L. Lai et al., *New parton distributions for collider physics*, *Phys. Rev.* **D 82** (2010) 074024 [arXiv:1007.2241] [INSPIRE].

[78] M. Ovchynnikov et al., *Coherent production of feebly interacting particles*, to appear.

[79] R.E. Shrock, *General Theory of Weak Processes Involving Neutrinos. 2. Pure Leptonic Decays*, *Phys. Rev.* **D 24** (1981) 1275 [INSPIRE].

[80] M.L. Perl, *The τ lepton*, *Rept. Prog. Phys.* **55** (1992) 653 [INSPIRE].

[81] E. Braaten, S. Narison and A. Pich, *QCD analysis of the tau hadronic width*, *Nucl. Phys.* **B 373** (1992) 581 [INSPIRE].

[82] S.G. Gorishnii, A.L. Kataev and S.A. Larin, *The $O(\alpha_s^3)$-corrections to $\sigma_{\rm tot}(e^+e^- \to hadrons)$ and $\Gamma(\tau^- \to \nu_\tau + hadrons)$ in QCD*, *Phys. Lett.* **B 259** (1991) 144 [INSPIRE].

[83] M. Antonelli et al., *Flavor physics in the quark sector*, *Phys. Rept.* **494** (2010) 197 [arXiv:0907.5386] [INSPIRE].

[84] F.J. Gilman and R.L. Singleton, *Analysis of semileptonic decays of mesons containing heavy quarks*, *Phys. Rev.* **D 41** (1990) 142 [INSPIRE].

[85] E. Blucher et al., *Status of the Cabibbo angle*, in the proceedings of the 3rd *International Workshop on the CKM Unitarity Triangle (CKM 2005)*, March 15–18, San Diego, California U.S.A. (2005), hep-ph/0512039 [INSPIRE].

[86] FlaviaNet Working Group on Kaon Decays collaboration, M. Antonelli et al., *Precision tests of the Standard Model with leptonic and semileptonic kaon decays*, in the

JHEP11(2018)032

proceedings of the *International Workshop on e^+e^- Collisions from ϕ to ψ (PHIPSI08)*, April 7–10, Frascati, Italy (2008), arXiv:0801.1817 [INSPIRE].

[87] BABAR collaboration, J.P. Lees et al., *Precise measurement of the $e^+e^- \to \pi^+\pi^-(\gamma)$ cross section with the initial-state radiation method at BABAR*, *Phys. Rev.* **D 86** (2012) 032013 [arXiv:1205.2228] [INSPIRE].

[88] L.M. Barkov et al., *Electromagnetic pion form-factor in the timelike region*, *Nucl. Phys.* **B 256** (1985) 365 [INSPIRE].

[89] CMD-2 collaboration, R.R. Akhmetshin et al., *High-statistics measurement of the pion form factor in the rho-meson energy range with the CMD-2 detector*, *Phys. Lett.* **B 648** (2007) 28 [hep-ex/0610021] [INSPIRE].

[90] KLOE collaboration, F. Ambrosino et al., *Measurement of $\sigma(e^+e^- \to \pi^+\pi^-)$ from threshold to 0.85 GeV^2 using Initial State Radiation with the KLOE detector*, *Phys. Lett.* **B 700** (2011) 102 [arXiv:1006.5313] [INSPIRE].

[91] KLOE collaboration, D. Babusci et al., *Precision measurement of $\sigma(e^+e^- \to \pi^+\pi^-\gamma)/\sigma(e^+e^- \to \mu^+\mu^-\gamma)$ and determination of the $\pi^+\pi^-$ contribution to the muon anomaly with the KLOE detector*, *Phys. Lett.* **B 720** (2013) 336 [arXiv:1212.4524] [INSPIRE].

[92] BESIII collaboration, M. Ablikim et al., *Measurement of the $e^+e^- \to \pi^+\pi^-$ cross section between 600 and 900 MeV using initial state radiation*, *Phys. Lett.* **B 753** (2016) 629 [arXiv:1507.08188] [INSPIRE].

[93] J.L. Rosner, S. Stone and R.S. Van de Water, *Leptonic decays of charged pseudoscalar mesons — 2015*, submitted to *Particle Data Book* (2015), arXiv:1509.02220 [INSPIRE].

[94] HPQCD collaboration, B. Colquhoun et al., *B-meson decay constants: a more complete picture from full lattice QCD*, *Phys. Rev.* **D 91** (2015) 114509 [arXiv:1503.05762] [INSPIRE].

[95] D. Ebert, R.N. Faustov and V.O. Galkin, *Relativistic treatment of the decay constants of light and heavy mesons*, *Phys. Lett.* **B 635** (2006) 93 [hep-ph/0602110] [INSPIRE].

[96] N. Dhiman and H. Dahiya, *Decay constants of pseudoscalar and vector B and D mesons in the light-cone quark model*, *Eur. Phys. J. Plus* **133** (2018) 134 [arXiv:1708.07274] [INSPIRE].

[97] D. Bečirević et al., *Lattice QCD and QCD sum rule determination of the decay constants of η_c, J/ψ and h_c states*, *Nucl. Phys.* **B 883** (2014) 306 [arXiv:1312.2858] [INSPIRE].

[98] R. Escribano, S. Gonzàlez-Solís, P. Masjuan and P. Sanchez-Puertas, *η' transition form factor from space- and timelike experimental data*, *Phys. Rev.* **D 94** (2016) 054033 [arXiv:1512.07520] [INSPIRE].

[99] S. Scherer, *Introduction to chiral perturbation theory*, *Adv. Nucl. Phys.* **27** (2003) 277 [hep-ph/0210398] [INSPIRE].

[100] T. Feldmann, *Quark structure of pseudoscalar mesons*, *Int. J. Mod. Phys.* **A 15** (2000) 159 [hep-ph/9907491] [INSPIRE].

[101] H. Leutwyler, *On the $1/N$ expansion in chiral perturbation theory*, *Nucl. Phys. Proc. Suppl.* **64** (1998) 223 [hep-ph/9709408] [INSPIRE].

[102] N.G. Deshpande and J. Trampetic, *Exclusive and semiinclusive B decays based on $b \to s\eta_c$ transition*, *Phys. Lett.* **B 339** (1994) 270 [hep-ph/9406393] [INSPIRE].

JHEP11(2018)032

[103] CLEO collaboration, K.W. Edwards et al., *Study of B decays to charmonium states $B \to \eta_c K$ and $B \to \chi_{c0} K$*, *Phys. Rev. Lett.* **86** (2001) 30 [hep-ex/0007012] [INSPIRE].

[104] C. Bourrely, I. Caprini and L. Lellouch, *Model-independent description of $B \to \pi l \nu$ decays and a determination of $|V_{ub}|$*, *Phys. Rev.* **D 79** (2009) 013008 [*Erratum ibid.* **D 82** (2010) 099902] [arXiv:0807.2722] [INSPIRE].

[105] HPQCD collaboration, H. Na et al., *$B \to D l \nu$ form factors at nonzero recoil and extraction of $|V_{cb}|$*, *Phys. Rev.* **D 92** (2015) 054510 [*Erratum ibid.* **D 93** (2016) 119906] [arXiv:1505.03925] [INSPIRE].

[106] S. Aoki et al., *Review of lattice results concerning low-energy particle physics*, *Eur. Phys. J.* **C 77** (2017) 112 [arXiv:1607.00299] [INSPIRE].

[107] O.P. Yushchenko et al., *High statistic study of the $K^- \to \pi^0 \mu^- \nu$ decay*, *Phys. Lett.* **B 581** (2004) 31 [hep-ex/0312004] [INSPIRE].

[108] NA48 collaboration, A. Lai et al., *Measurement of $K_0(\mu 3)$ form factors*, *Phys. Lett.* **B 647** (2007) 341 [hep-ex/0703002] [INSPIRE].

[109] ETM collaboration, V. Lubicz et al., *Scalar and vector form factors of $D \to \pi(K) \ell \nu$ decays with $N_f = 2 + 1 + 1$ twisted fermions*, *Phys. Rev.* **D 96** (2017) 054514 [arXiv:1706.03017] [INSPIRE].

[110] G. Duplancic and B. Melic, *Form factors of B, $B_s \to \eta^{(\prime)}$ and D, $D_s \to \eta^{(\prime)}$ transitions from QCD light-cone sum rules*, *JHEP* **11** (2015) 138 [arXiv:1508.05287] [INSPIRE].

[111] C.J. Monahan et al., *$B_s \to D_s \ell \nu$ form factors and the fragmentation fraction ratio f_s/f_d*, *Phys. Rev.* **D 95** (2017) 114506 [arXiv:1703.09728] [INSPIRE].

[112] D. Melikhov and B. Stech, *Weak form-factors for heavy meson decays: an update*, *Phys. Rev.* **D 62** (2000) 014006 [hep-ph/0001113] [INSPIRE].

[113] D. Ebert, R.N. Faustov and V.O. Galkin, *New analysis of semileptonic B decays in the relativistic quark model*, *Phys. Rev.* **D 75** (2007) 074008 [hep-ph/0611307] [INSPIRE].

[114] R.N. Faustov and V.O. Galkin, *Relativistic description of weak decays of B_s mesons*, *AIP Conf. Proc.* **1701** (2016) 050020 [arXiv:1411.7232] [INSPIRE].

[115] N. Mathur, M. Padmanath and R. Lewis, *Charmed-bottom mesons from lattice QCD*, *PoS* **LATTICE2016** (2016) 100 [arXiv:1611.04085] [INSPIRE].

[116] L.N. Chang, O. Lebedev and J.N. Ng, *On the invisible decays of the Υ and J/Ψ resonances*, *Phys. Lett.* **B 441** (1998) 419 [hep-ph/9806487] [INSPIRE].

[117] HERA-B collaboration, I. Abt et al., *Measurement of D^0, D^+, D_s^+ and D^{*+} production in fixed target 920 GeV proton-nucleus collisions*, *Eur. Phys. J.* **C 52** (2007) 531 [arXiv:0708.1443] [INSPIRE].

[118] C. Lourenco and H.K. Wohri, *Heavy flavour hadro-production from fixed-target to collider energies*, *Phys. Rept.* **433** (2006) 127 [hep-ph/0609101] [INSPIRE].

[119] G.J. Gounaris and J.J. Sakurai, *Finite width corrections to the vector meson dominance prediction for $\rho \to e^+ e^-$*, *Phys. Rev. Lett.* **21** (1968) 244 [INSPIRE].

JHEP11(2018)032